Elsevier Editorial System(tm) for Molecular Catalysis

Manuscript Draft

Manuscript Number: MOLCAA-D-19-00462R2

Title: Versatile Titanium Dioxide Nanoparticles prepared by Surface-Grown Polymerization of Polyethylenimine for Photodegradation and Catalytic C-C Bond Forming Reactions

Article Type: Research Paper

Section/Category: Heterogeneous catalysis

Keywords: Polyethylenimine polymer, Titanium dioxide, Photocatalytic degradation, Knoevenagel condensation, Multicomponent reactions

Corresponding Author: Dr. Yolanda Pérez Cortés,

Corresponding Author's Institution:

First Author: Josefa Ortiz-Bustos

Order of Authors: Josefa Ortiz-Bustos; Mariano Fajardo; Isabel del Hierro; Yolanda Pérez Cortés

Abstract: Crystalline TiO2 anatase nanoparticles have been synthesized by a sol-gel procedure with a certain ratio of brookite phase due to low calcination temperature. TiO2 NPs have been successfully functionalized with hyperbranched polyethylenimine polymer (PEI) by the surface polymerization of aziridine or with N1-(3-trimethoxysilylpropyl)-diethylenetriamine (DT) by surface silanization to form catalyst with notable basic and photocatalytic properties. The TiO2 NPs have been characterized by X-ray diffraction (XRD), adsorption-desorption isotherms, fourier-transform infrared spectroscopy (FT-IR), diffuse reflectance UV-Vis spectroscopy (DRUV-vis), elemental analysis, thermogravimetric analysis, transmission electron microscopy (TEM) and solid-state voltammetry. Functionalized TiO2 NPs have revealed to be efficient in the photodegradation of methylene blue in water and as basic heterogeneous catalysts carbon-carbon forming reactions as Knoevenagel condensation, multicomponent reactions and Biginelli reaction. PEI-TiO2 with mesoporous structure and narrow size pore distribution, fulfill the requirements imposed to an eco-friendly and cost-effective catalyst since it is easily synthesized and recyclable.

First of all, we would like to thank the reviewer comments since we consider they deeply improve the quality of our work. The appropriate modifications have been included.

Reviewer #1: Authors have properly answered the questions in the revised version. Hence, this paper can be accepted in Molecular Catalysis after following modifications:

1- In scheme 2, CO2 should be CO_2 (subscript)

The word "CO_2" has been corrected in the Scheme 2.

2- Some recent reference on photocatalytic application of TiO2 for organic reaction should be cited, Molecular Catalysis 458 (2018) 33-42.; Molecular Catalysis 452 (2018) 175-183.; Molecular Catalysis 471 (2019): 71-76.; Molecular Catalysis 465 (2019): 16-23.

The references have been included in the text.

*Graphical Abstract

Graphical Abstract

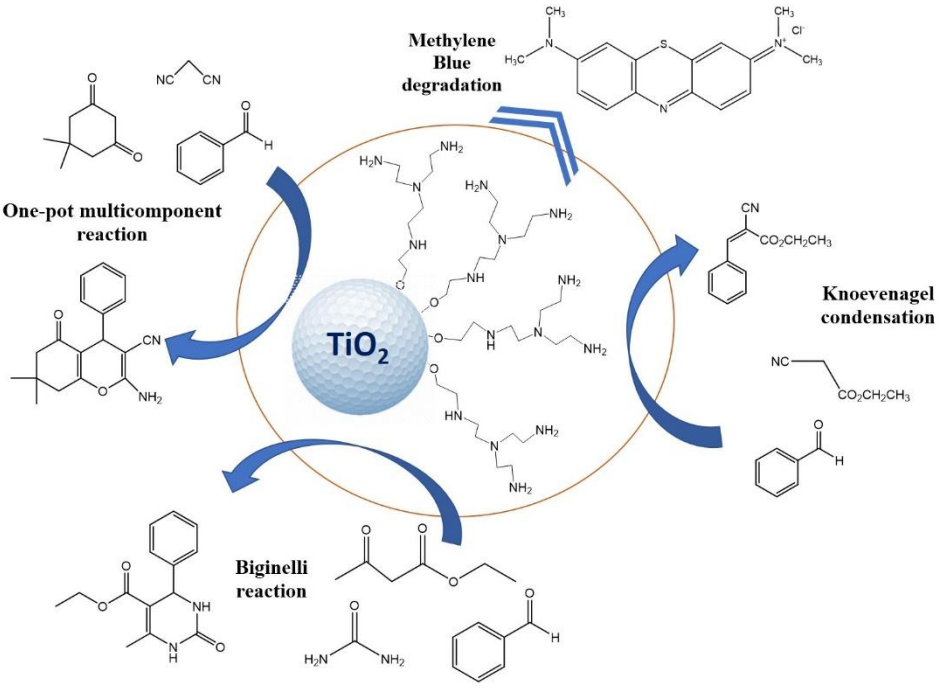

Highlights

- Functionalized titanium dioxide nanoparticles as versatile catalysts.
- Highly efficient in the photodegradation of methylene blue in water and as basic catalysts in Knoevenagel condensation and multicomponent reactions.
- Study of the electrochemical properties of titanium dioxide samples using cyclic voltammetry

Versatile Titanium Dioxide Nanoparticles prepared by Surface-Grown Polymerization of Polyethylenimine for Photodegradation and Catalytic C-C Bond Forming Reactions

Josefa Ortiz-Bustos[a], Mariano Fajardo[a], Isabel del Hierro[a]*, Yolanda Pérez[a]*
Departamento de Biología y Geología, Física y Química Inorgánica. Escuela Superior de Ciencias Experimentales y Tecnología. Universidad Rey Juan Carlos. 28933 Móstoles (Madrid), Spain. Tel.: (+34) 916647444
E-mail: yolanda.cortes@urjc.es

Abstract

Crystalline TiO_2 anatase nanoparticles have been synthesized by a sol-gel procedure with a certain ratio of brookite phase due to low calcination temperature. TiO_2 NPs have been successfully functionalized with hyperbranched polyethylenimine polymer (PEI) by the surface polymerization of aziridine or with N^1-(3-trimethoxysilylpropyl)-diethylenetriamine (DT) by surface silanization to form catalyst with notable basic and photocatalytic properties. The TiO_2 NPs have been characterized by X-ray diffraction (XRD), adsorption-desorption isotherms, fourier-transform infrared spectroscopy (FT-IR), diffuse reflectance UV-Vis spectroscopy (DRUV-vis), elemental analysis, thermogravimetric analysis, transmission electron microscopy (TEM), photoluminiscence spectroscopy (PL) and solid-state voltammetry. Functionalized TiO_2 NPs have revealed to be efficient in the photodegradation of methylene blue in water and as basic heterogeneous catalysts carbon-carbon forming reactions as Knoevenagel condensation, multicomponent reactions and Biginelli reaction. PEI-TiO_2 with mesoporous structure and narrow size pore distribution, fulfill the requirements imposed to an eco-friendly and cost-effective catalyst since it is easily synthesized and recyclable.

Keywords: Polyethylenimine polymer, Titanium dioxide, Photocatalytic degradation, Knoevenagel condensation, Multicomponent reactions.

1. Introduction

Titanium dioxide is a low cost, non-toxic, corrosion resistant and biocompatible material which possesses important applications in biology [1], medical [2], solar cells [3], CO_2 reduction [4], water splitting [5], degradation of pollutants [6], selective oxidation [7] and synthesis of organic chemicals [8-11]. These applications are affected by parameters such as specific surface area, particle size distribution and porous structure, etc. [12]. In particular, the photocatalytic activity is strongly affected by crystalline structure, since the enhancement of the photocatalytic efficiency can occur by altering the electronic band structure of titanium dioxide [13]. Different approaches are found in the literature to enhance the photocatalytic activity of TiO_2 and to improve its efficiency in pollutant degradation procedures under UV or visible light irradiation, prevailing doping methodologies, with non-metals [14] or metal ions [15] and with two or more elements (co-doping) [16], and sensitization of TiO_2 with organic compounds [17, 18].

The modification of TiO_2 with organic ligands improves the dispersion of the nanoparticles of TiO_2 in water or organic solvents and it may increase the adsorption of organic pollutants on the photocatalyst's surface. This modification on TiO_2 involves physical adsorption such as van der Walls forces, hydrophobic or electrostatic interactions, hydrogen bonding and covalent bonding. The covalent bond formation, between Ti-O-H groups and the ligands employed for the functionalization, increases the stability of the coverage, led to minimal desorption and provides a more even distribution of the organic compounds to form monolayer coverages [19]. The modification of TiO_2 by post-synthesis grafting is limited due to the low amount of hydroxyl groups on the surface, that is why grafting method has been reported to be efficient only with some ligands, among them, organosilanes, organophosphates and carboxylic acid derivatives [19]. Li et al. [20] prepared functionalized TiO_2 nanoparticles using surface modification method over TiO_2 with 3-aminopropyltriethoxysilane as silane coupling agent. The mass percentage of organic functionality on TiO_2 was calculated by thermogravimetric analysis resulting 3.21%. Weerachawanasak et al. [21] functionalized TiO_2 with varying amounts of 3-aminopropyltriethoxysilanye using post-synthesis grafting method and the quantitative line scan analysis by SEM showed amounts of Si between 0.5-1.1%. Zhao et al. [22] modified commercial TiO_2 with organosilanes in water. They calculated the incorporation of organosilanes on TiO_2 by thermal gravimetric analysis which was much higher for 3-isocyanatopropyltrimethoxysilane grafted TiO_2 nanoparticles (27.4%) than that for 3-aminopropyltrimethoxysilane grafted TiO_2 nanoparticles (2.4%). They concluded that this fact was due to the cross-linked net formed by 3-isocyanatopropyltrimethoxysilane attached to TiO_2 nanoparticles. These modified TiO_2 nanoparticles was tested in the photodegradation of dye malachite green. They detected that photocatalytic activity was dependent on the grafting efficiency, when

the amount of organosilane increased, the rate constant tended to decrease. Ziarati et al. [23] functionalized yolk@shell TiO_2 structures with N-(2-aminoethyl)-3-aminopropyltriethoxysilane for the synthesis of graphene highly wrapped yolk@shell TiO_2 photocatalyst. The introduction of silane ligand agent improves the interaction of GO with yolk@shell TiO_2.

In this manuscript, the functionalized titanium dioxide nanoparticles by surface-grown polymerization of polyethylenimine using aziridine as monomer is described. The PEI is a polymer that possesses a high amount of basic groups (primary, secondary and tertiary amines) which lead to the capture of protons by PEI polymer. This polymer helps to improve the dispersion and stability of the TiO_2 material [24] and also increases electron mobility and reduces series resistance [25]. The polymer grows on Ti-OH groups of the surface of TiO_2 nanoparticles resulting 15.9% of organic content attached to the surface of TiO_2 nanoparticles as calculated by thermogravimetric analysis. For comparison purposes, the commercially available N^1-(3-trimethoxysilylpropyl)diethylenetriamine (DT) was also anchored post-synthesis onto TiO_2 nanoparticles rendering lower organic contents. PEI and DT modified TiO_2 nanoparticles have been tested in the photodegradation of methylene blue (MB) in aqueous solution under UV irradiation obtaining higher degradation efficiency in comparison with unmodified TiO_2 material. In addition, they have demonstrated to be highly dispersed in polar and non-polar solvents. Since the compounds used in this work are amino based ligands [26], we have also tested them as basic catalysts in C-C bond formation reactions of interest (Knoevenagel condensation, multicomponent reactions and Biginelli reaction) [27, 28] as eco-friendly and versatile catalysts. The electrochemical properties of TiO_2 samples have investigated using cyclic voltammetry. Thus, the nature of the ligand and the functionalization procedure provide each material, PEI-TiO_2 and DT-TiO_2, their own characteristics as demonstrated in this work.

2. Experimental Section

2.1. Materials

Titanium (IV) isopropoxide ≥ 97%, N^1-(3-trimethoxysilylpropyl)diethylenetriamine 85%, ethyl cyanoacetate 99%, malononitrile 99%, urea 99%, 5,5-dimethylcyclohexane-1,3-dione 99%, benzaldehyde 99.5%, and nitric 65% and acetic acids were purchased from Sigma Aldrich. Thiourea 99% and ethyl acetoacetate 99% were purchased from Across and stabilized aziridine from Menadiona (Spain). Methylene blue was purchased from Scharlab. Solvents were acquired from SDS; toluene and dichloromethane were distilled and dried from drying agents and ethanol and 2-propanol were used as received.

2.2. Preparation of catalyst

2.2.1. Synthesis of TiO_2 nanoparticles

TiO_2 mesoporous material was prepared following a procedure developed by our group previously [12] with a slight modification. In a typical synthesis, titanium (IV) isopropoxide (40 mL) were dissolved in dry 2-propanol (2:5). Then, a solution of nitric acid in milliQ water at pH 2 was added dropwise to the solution with a peristaltic pump. The suspension was stirred vigorously for 16 hours and then it was filtered off. The white solid was dried at 90 ^{o}C and calcined in air at 400 ^{o}C for 16 hours.

2.2.2. Functionalization of TiO_2 nanoparticles by polymerization of aziridine (PEI-TiO_2)

Prior to the reaction, 1.5 g of TiO_2 material was dehydrated under vacuum at 80 °C for 5 h. In a post-synthetic method [29], the polymerization of aziridine was performed onto the surface Ti-OH groups of the TiO_2 material. TiO_2 support was suspended in 40 mL of dry toluene with stirring and under nitrogen atmosphere. After, 75 µL of acetic acid and 750 µL of stabilized aziridine was added and the suspension was stirred for 10 h at 75 °C. Finally, the suspension was filtered off and washed with toluene and methanol. The resulting solid was dried under vacuum and denoted as PEI-TiO_2.

2.2.3. Functionalization of TiO_2 nanoparticles by grafting of N^1-(3-trimethoxysilylpropyl)diethylenetriamine (DT-TiO_2)

Like the previous synthesis, as-synthesized TiO_2 was dehydrated under vacuum at 120 °C for 5 h to remove residual physisorbed water. Then, surface modification of TiO_2 was carried out by post-synthesis grafting, where 1 g of TiO_2 was suspended in 50 mL of dry toluene and 10% molar ratio of N^1-(3-trimethoxysilylpropyl)diethylenetriamine was added. The reaction was kept under nitrogen atmosphere and stirring at 110 °C (reflux) for 48h. The suspension was filtered and the resultant solid washed with toluene. Finally, the solid was dried under vacuum and labelled as DT-TiO_2.

2.3. Characterization Techniques

X-Ray diffraction (XRD) patterns of the materials were acquired on a Phillips Diffractometer model PW3040/00 X'Pert MPD/MRD at 45 KV and 40 mA, using Cu-Kα radiation (λ=1.5418 Å). Adsorption-desorption isotherms of nitrogen were recorded using a Micromeritics TriStar 3000 analyser. FT-IR spectra were performed on a Varian

Excalibur Series 3100 – UMA 600 spectrometer (in the region 4000 to 400 cm^{-1}) in Attenuated Total Reflectance (ATR) mode. ^{1}H NMR and ^{13}C NMR spectra were recorded on a Varian Mercury FT-400 spectrometer. Thermogravimetric analysis was obtained with a Setsys 18 A (Setaram) analyzer. DRUV-Vis spectra were performed using a Varian Cary 500 spectrophotometer in diffuse reflectance mode. Transmission electron microscope (TEM) pictures were acquired using JEOL JEM1010 working at 100 kV. The zeta potencial values of samples was calculated by suspending of nanoparticles in a buffered solution (0.1 mg ml^{-1}) at pH 7.3 using Nanoplus Zeta Potential and Nano Particle Analyzer from Micromeritics. The electrochemical studies were carried out with a potentiostat/galvanostat Autolab PGSTAT302 Metrohm. Solid-state emission spectra were measured on a Perkin-Elmer LS 55 fluorescence spectrometer with a Xe lamp at 250 nm excitation wavelength. The data were collected at every 0.5 nm. Slit widths for excitation and emission were 10 nm.

2.4. Modified Carbon Paste Electrode Preparation

To prepare the modified carbon paste electrode used as working electrode a fixed amount of graphite (electrochemistry quality, Metrohm) and the titanium oxide nanoparticles under study are firstly mixed (10% TiO_2/graphite (w,w)) with a pestle in an agate mortar and, finally, the mixture is agglutinated by using nujol or mineral oil. The so prepared carbon paste was packed into the end part of a Teflon tube with a screwing stainless-steel piston to provide an inner electrical contact. The initial carbon paste electrode activity can be easily restored by polishing the outer surface of paste with a soft paper.

3. Catalytic experiments

3.1. Photocatalytic degradation of aqueous Methylene Blue (MB).

Photocatalytic reactions were carried out under UV irradiation at 365 nm and 36 W (4 × 9 W). In this condition, 20 mg of the TiO_2 sample was dispersed in 50 mL of 0.04 mM MB solution. In a previous step, suspension with the TiO_2 sample was stirred for 1 h to assure the saturation of the surface of the TiO_2 (adsorption – desorption equilibrium). The photodegradation of MB was studied using a spectrophotometer (SP-830) at 664 nm, which is the maximum of the MB absorbance. Each experiment was performed by duplicate and measuring the absorbance in triplicate.

3.2. Knoevenagel Condensation Reaction

TiO_2 sample (50 mg) was suspended in 5 mL of solvent (see Table 3) and benzaldehyde (11 mmol) and malononitrile or ethyl cyanoacetate (11 mmol) were added in a 50 mL tube. The mixture was stirred at room temperature or heated at 60 °C. After the reaction time, diethyl ether (5 mL) were added to the mixture and the catalyst was precipitated and separated by centrifugation. The liquid phase was analyzed by GC-FID (Agilent 6890N, DB-Wax capillary column 30 m, 0.53 mm) using dodecane as external standard. The products obtained were purified by recrystallization in acetone and analyzed by NMR spectroscopy (see supplementary material). The catalyst was washed with ethanol (3 x 5 mL) and dried and recycled several times under the same conditions.

3.3. One pot condensation reaction

In this reaction, TiO_2 sample (25 mg) was dispersed in 5 mL of ethanol and malononitrile (5.5 mmol), benzaldehyde (5.5 mmol) and 5,5-dimethylcyclohexane-1,3-dione (5.5 mmol) were added in a 50 mL tube. The suspension was stirred at room temperature. After the reaction time, diethyl ether (5 mL) were added to the mixture and the catalyst was precipitated and separated by centrifugation. The chromene obtained was purified by recrystallization in ethanol and analyzed by NMR spectroscopy (see supplementary material).

3.4. Biginelli reaction

This condensation reaction consists on the synthesis of 3,4-dihydropyrimidinone (or thione) obtained in solvent less condition or using ethanol as solvent. Thus, ethyl acetoacetate (1 mmol), benzaldehyde (1 mmol) and urea or thiourea (1.2 mmol) were mixed in a schlenk tube. To this mixture, 50 mg of PEI-TiO_2 catalyst was added and then heated at 80 ^{o}C for 2 h. After cooling, ethanol was added to the mixture and the catalyst was separated by centrifugation. The product was recrystallized from ethanol and analyzed by NMR spectroscopy (see supplementary material).

4. Results and Discussion

4.1. Synthesis and Characterization

In this study, TiO_2 nanoparticles were synthesized by hydrolysis of titanium (IV) isopropoxide at pH 2 following the methodology reported by our group [30], but the calcination temperature was dropped to 400 °C in order to obtain mesoporous titanium oxide nanoparticles with high specific surface area and uniform mesopores. The surface polymerization of aziridine was carried out in toluene as solvent at 75 °C to obtain hyperbranched polyethylenimine polymer (PEI) covalently attached to TiO_2 (PEI-TiO_2) through Ti-O-C bond formation (Scheme 1). Polyethylenimine (PEI) is a polymer which possesses reactive primary, secondary and tertiary amino groups, with different pK_a values, which can capture protons at different pH conditions [31]. For comparison purposes, the commercially available N^1-(3-trimethoxysilylpropyl)diethylenetriamine (DT) was also anchored post-synthesis onto TiO_2 nanoparticles and the material obtained was labelled hereafter as DT-TiO_2.

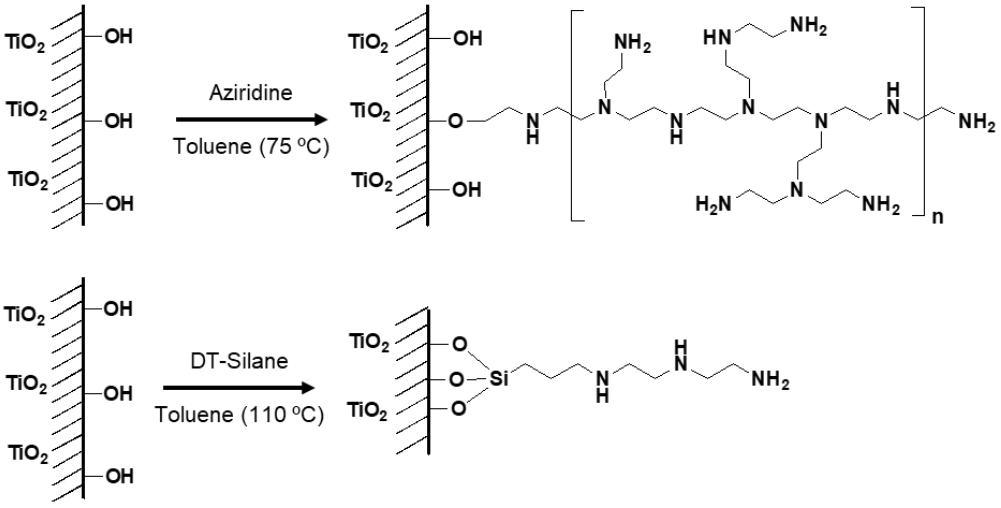

Scheme 1. Hyperbranching polymerization of aziridine onto TiO_2 NPs surface (PEI-TiO_2) and silanization with N^1-(3-trimethoxysilylpropyl)diethylenetriamine (DT-TiO_2)

The TiO_2 samples were characterized by powder XRD detecting that they are crystalline materials (Fig. 1). Although anatase is the main crystal phase, additional peaks of brookite phase appeared. To study in more detail the brookite phase, the peaks with Miller indexes (121) and (120) must be taken into account, since the peak (120) due also to brookite appears overlapped with the strongest diffraction peak (101) of anatase. Ideal brookite has a $I_{brookite}$ (121)/$I_{brookite}$ (120) ratio of ~0.9, as shown by the diffraction data file (JCPDS: 21-1276) [32], so the amount of brookite in the material synthetized in this work might be estimated from the $I_{brookite}(121)$ /($I_{brookite}$ (120) + $I_{anatase}$ (101)) [32] ratio as 26% for pure TiO_2 and 20% and 19.8% for functionalized PEI and DT-TiO_2 samples, respectively. As can be seen, the amount of the anatase increased slightly upon functionalization which can be due to the additional ageing time during organic incorporation. The crystal shape was study by transmission

electron microscopy and X-ray diffraction. TEM representative images and corresponding size distribution histograms of TiO_2 and PEI-TiO_2 nanoparticles are shown in Fig. 2. An aggregation of roughly round particles is observed for pristine TiO_2 with particle size of 11.07 nm (with narrow size distribution). Meanwhile, after PEI-TiO_2 functionalization, a significant decrease of the nanoparticle's aggregation and a slight increase of the particle size to 11.88 nm and particle size distribution take place. Durupthy and coworkers [33] have used the lines (101, 004, and 200) of XRD patterns to estimate the crystal shape of TiO_2 since these lines shown to correspond to the more displayed faces ((101), (001) and 100) in natural anatase crystals. In our XRD measured pattern the line 101 of anatase overlaps with line 102 for brookite phase and makes impossible a precise estimation of the crystal shape based on these measurements. However, mean size *d* of anatase nanoparticles in TiO_2, PEI-TiO_2 and DT-TiO_2 shows in all cases $d_{[200]} > d_{[004]}$ supporting the formation of roughly round anatase nanoparticles with an homogeneous particle size distribution as observed by TEM studies (Fig. 2). The crystallite size was estimated by the Scherrer's equation resulting in a grain size of 8.36 nm for unmodified TiO_2 nanoparticles and increasing to 8.85 and 8.93 nm after functionalization with PEI and DT ligands, respectively (Fig. 2).

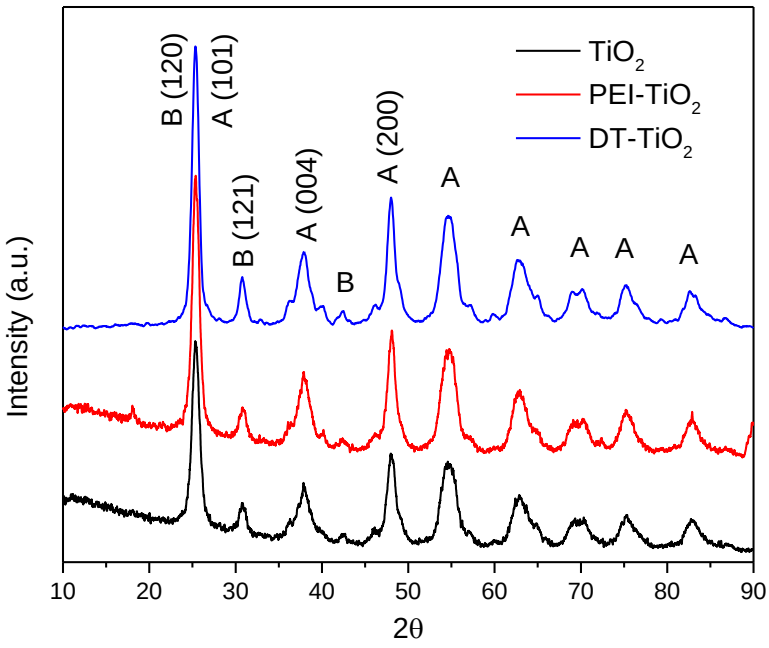

Fig. 1. X-Ray diffractograms of TiO_2, PEI-TiO_2 and DT-TiO_2 (A=Anatase, B=Brookite)

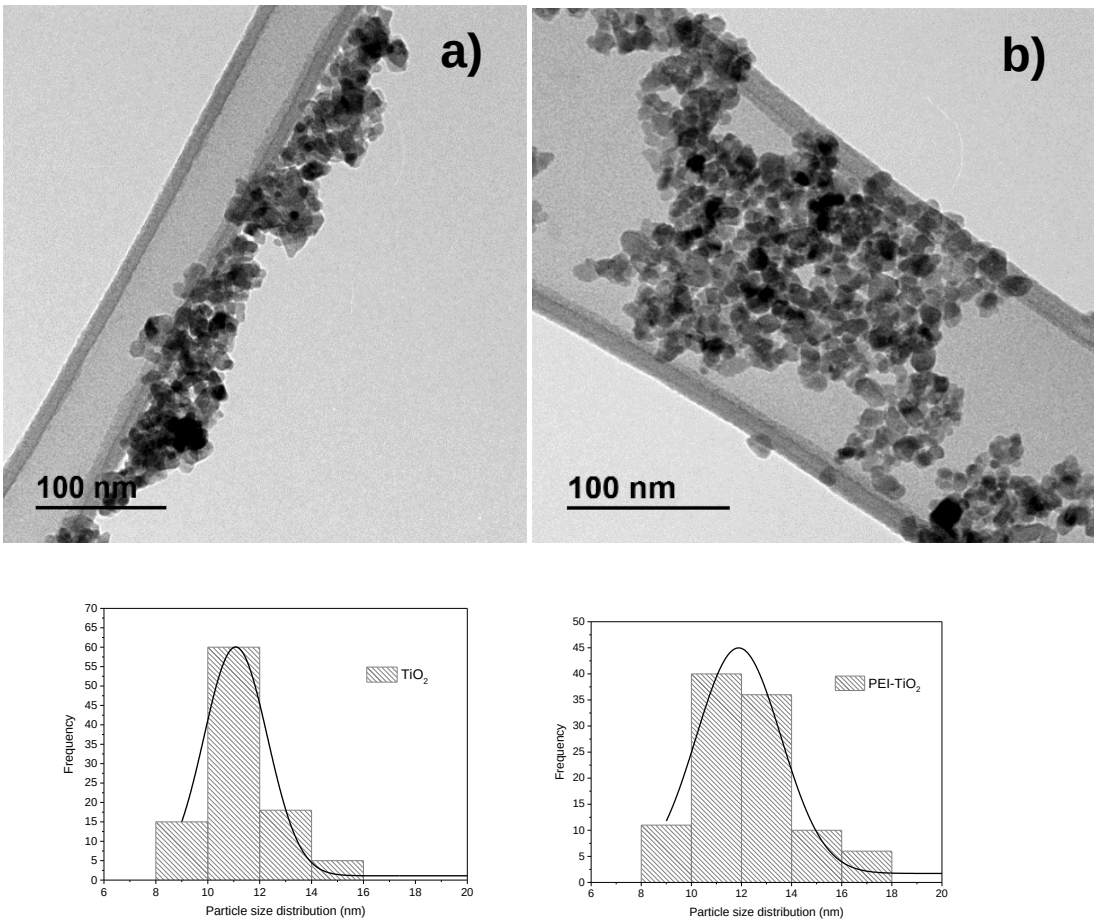

Fig. 2. TEM micrographs and size distribution histograms of a) TiO_2 and b) PEI-TiO_2.

The textural properties were measured by adsorption-desorption experiments. Adsorption-desorption isotherms of TiO_2 and functionalized TiO_2 samples are displayed in Fig. 3. All materials exhibit type IV isotherms typical of mesoporous materials in accordance with the IUPAC classification. Pronounced desorption hysteresis indicates the presence of large mesopores in the TiO_2 nanoparticles. This hysteresis is between H1 and H2-type hysteresis loop from 0.40 to 0.90 relative pressure, which suggest the existence of an assembly of uniform mesopores, cage like type, interconnected by bottleneck channels [34, 35].The functionalized PEI and DT-TiO_2 materials cause a decrease in the specific surface area and pore volume values in comparison with the parent TiO_2, which suggests a successful incorporation of PEI polymer and DT ligand in PEI-TiO_2 and DT-TiO_2 materials, respectively (Table 1). BJH pore size distributions are 8.0, 7.9 and 7.3 nm, for TiO_2 and for PEI-TiO_2 and DT-TiO_2, respectively (Fig. S1). The quantity of molecules attached to DT-TiO_2 was calculated by elemental analysis being L_o = 0.40 mmol g^{-1} (L_o = %N/3×nitrogen molecular weight). Considering L_o and S_{BET} of DT-TiO_2 material, the average surface density (d) of grafted molecules and the average intermolecular distance were estimated as 3.36 molecules/nm^2 and 0.54 nm, respectively. Similarly, the amount of PEI grafted to the PEI-TiO_2 was estimated as 2.36 mmol of amine groups per gram of material, the surface density of the amino groups of PEI was calculated as 15.33 amino groups/nm^2 and because of the high degree of

PEI grafting, the distance between these amino groups was only 0.26 nm [36]. Thermogravimetric analysis (TGA) of functionalized sample, PEI-TiO_2 (Fig. 4), reveals two weight losses. The first loss which occurs from 25 °C to 200 °C and can be due to physisorbed water. The second one is observed above 210 °C and corresponds to the decomposition of the organic species. There is no PEI degradation before 200 °C which is consistent with the covalent immobilization of PEI to the hydroxyl surface groups [29]. The total weight loss percentage of 15.9% supports the existence of a high organic content attached to the surface of TiO_2 nanoparticles in PEI-TiO_2 material. Similarly, TGA for DT-TiO_2 shows the degradation of covalently attached organosilanes functional groups between 200 and 450 °C (Fig. 4).

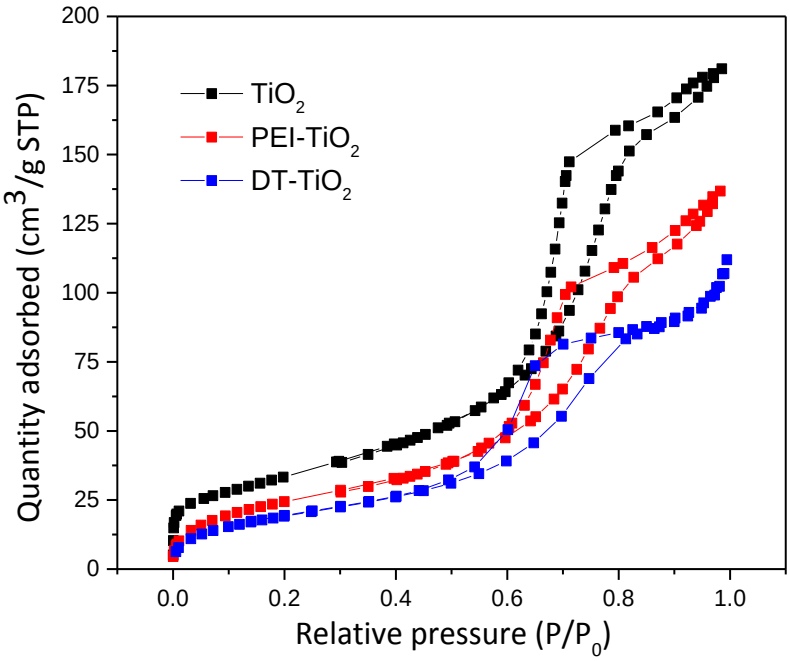

Fig. 3. Adsorption-desorption isotherms of TiO_2, PEI-TiO_2 and DT-TiO_2

Table 1. Properties of TiO_2 samples

Material	S_{BET} ($m^2.g^{-1}$)	V_p[a] ($cm^3.g^{-1}$)	D_p[a] (nm)	Organic content (%)[b]	N Content (mmol N/g)[c]	Surface Coverage (nm^{-2})	Particle size (nm)[d]	Band gap (eV)
TiO_2	120.3	0.28	8.0	-	-		8.36	3.09
PEI-TiO_2	92.6	0.21	7.9	15.9	2.36	15.33	8.85	3.18
DT-TiO_2	72.4	0.18	7.3	7.7	1.21	3.37	8.93	3.19

[a] Pore size and pore volume as determined by the BJH method from the adsorption of the nitrogen isotherm

[b] Organic content determined by TGA

[c] Nitrogen content determined by elemental analysis

[d] Determined by Scherrer's equation

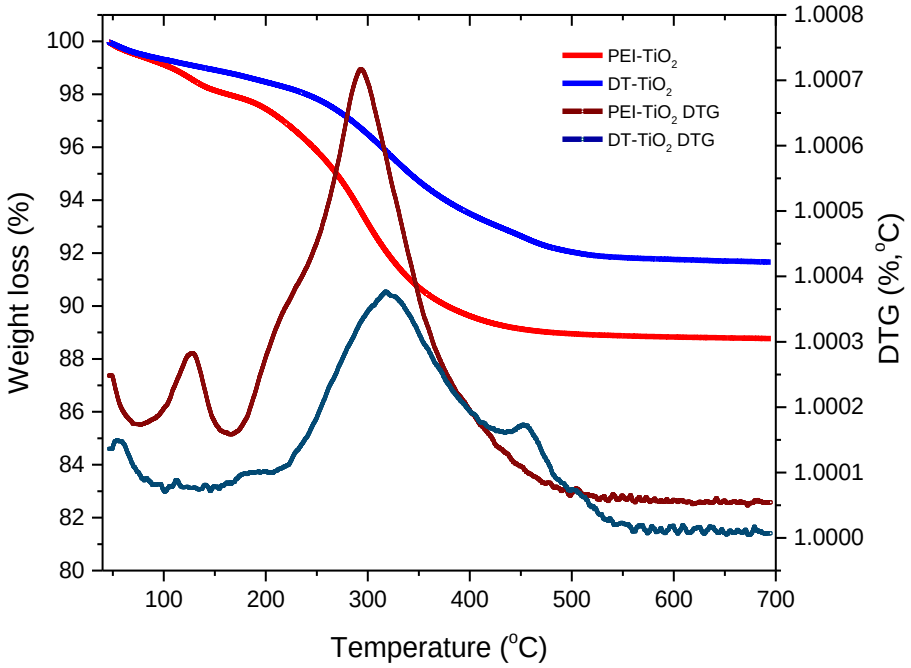

Fig. 4. TGA and DTG curves of PEI-TiO_2 and DT-TiO_2 materials

FT-IR spectra were recorded to confirm the functionalization of TiO_2 nanoparticles. Fig. 5 shows the FT-IR spectra of TiO_2 samples. The spectra show a type broad band in the range 950-400 cm^{-1} associated to Ti-O and Ti-O-Ti bonds. For all the samples, the stretching vibrations of physiosorbed water are observed between 3400 and 3200 cm^{-1}, overlapping with that of surface Ti-OH groups of the TiO_2, and by the medium band at 1632 cm^{-1} associated to deformation vibrations of adsorbed water molecules. In the FT-IR spectrum of PEI-TiO_2 a significant decrease is observed for the band corresponding to the Ti-O-H surface groups indicating their involvement in the PEI attachment reaction. New bands, associated to hyperbranched PEI polymer, as observed by comparison with free PEI (Fig. S2), appear at 2933 and 2821 cm^{-1} for ν(C–H) stretching vibrations and at 1421 cm^{-1} for bending vibrations of methylene groups. The band due to δ(N–H) bending vibration of primary amines, which is observed at 1560 cm^{-1} [37]. In the case of N^1-(3-trimethoxysilylpropyl)diethylenetriamine the decrease observed for the band in the range 3400 and 3200 cm^{-1} due to hydroxyls groups onto TiO_2 surface confirms the chemisorption of amino silane molecules via the formation of a covalent Ti-O-Si bond. The bands from 2928 to 2811 due to ν(C-H) bonds, whereas the bands at 1468 and 1407 cm^{-1} are attributed to δ(C-H) bending and ν(C-N), respectively. Finally, the bending vibrations associated to secondary and primary amine groups are supported by peaks at 1574 and 1650 cm^{-1}. With DT as

silylating agent and taking into account the presence of Ti-O-H onto the anatase phase, with OH's acidic groups and Lewis acid Ti^{4+} sites, the existence of additional interactions trough the nitrogen lone-pair of amino groups (Ti^{4+}--:NH_2-/Ti-O-H--:NH_2-) cannot be discarded. This proposal is supported by the elegant study performed by Zaki and coworkers who developed a complete FTIR in situ study of pyridine adsorption on different oxides, among them, TiO_2. This work concluded the formation, at room temperature, of nitrogen lone pair interactions with Ti^{4+} acid sites, as well as, H-bonding molecules (Py:---H-O-Ti) [38]. The behaviour of APTES (aminopropyltriethoxisilane) as silylating agent of a wide amount of silica materials is also well know. Different authors have proposed the formation of hydrogen bonds between NH_2 groups and water molecules allowing the protonation of the amine, since additional bands attributed to asymmetric $–NH_3^+$ deformation mode are clearly visible in their FTIR spectra. In this regard, the FTIR spectrum of DT-TiO_2 shows an additional band at 1561 cm^{-1} that could be equally associated to the formation of $–NH_3^+$ groups by protonation of the amine groups in the presence of acidic OH's (Ti-O^---:NH_3^+-) (Fig. 5 and S3). The thermogravimetric analysis for DT-TiO_2 can also be informative, the percentage weight loss observed below 200 ^oC, usually attributed to physiosorbed water, decreases smoothly in this range of temperature on the contrary to that observed for PEI-TiO_2 where a more pronounced weight loss is observed between 50 and 150 ^oC. In addition, the DTG calculated for DT-TiO_2 shows two small and differentiate peaks below 150 and below 200 ^oC, respectively. This thermogravimetric analysis could be explained by the consecutive desorption of water (lower % moisture loss than PEI-TiO_2) and non-covalently attached DT (Fig. 4). Since in this work the material has been thoroughly washed during the functionalization procedure, we proposed based on this thermogravimetric analysis the existence of a low amount of non-covalently DT physisorbed onto TiO_2. This is consistent also with previous results which indicate that a fixed amount of amino silane, between 3-10%, remains physisorbed even after exhaustive rinsing procedures [39].

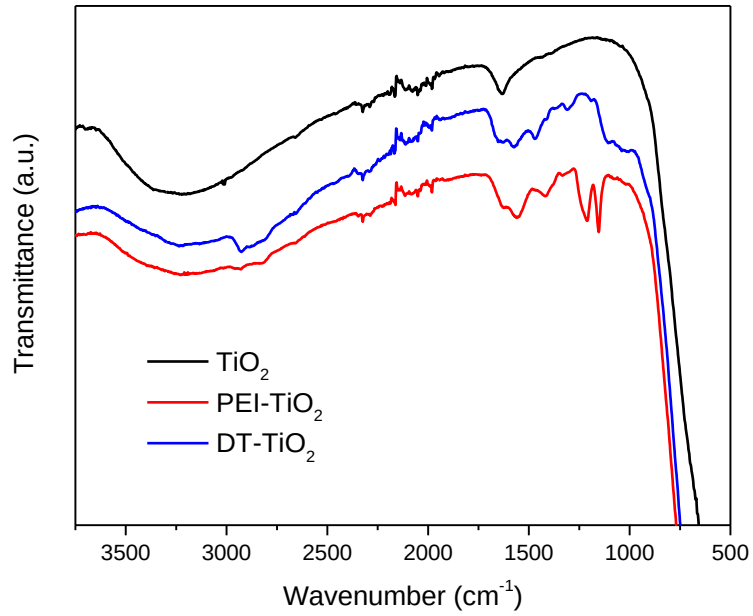

1

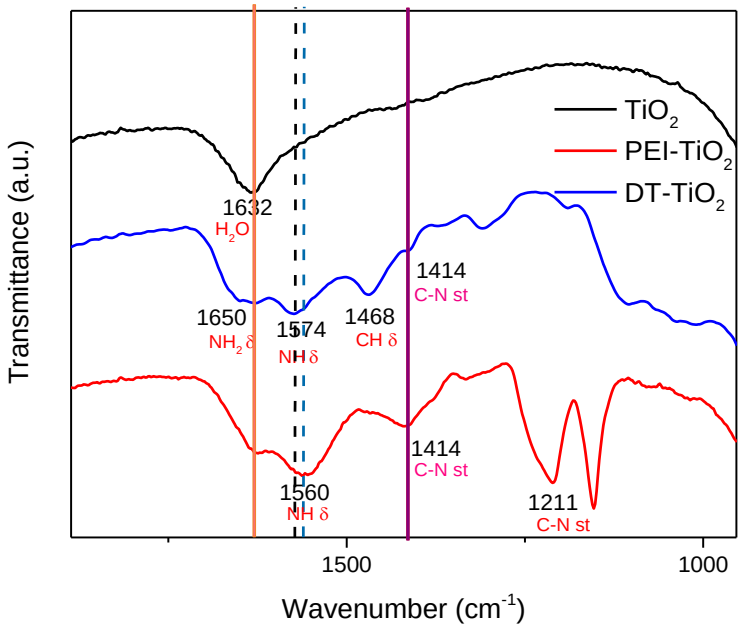

2

3 Fig. 5. FTIR spectra of TiO_2 and functionalized PEI-TiO_2 and DT-TiO_2 materials.

4 The DRUV-Vis spectra of bare and functionalized TiO_2 synthesized samples are shown
5 in Fig. 6. The reflectance data shows a broad band and are characteristic of this type of
6 materials, with an absorbance maximum around 320 nm associated to band-band
7 transition. For PEI-TiO_2 a second peak is observed at 230 nm attributed to the
8 existence of the hyperbranched PEI polymer attached to the surface of TiO_2, as can be
9 deduced from comparison with the spectra recorded for PEI in solution (Fig. S4). Also,

as can be seen, a blue shift is observed after organic functionalization. The extrapolated line draw calculated by the application of the Kubelka-Munk algorithm (Fig. S3) from the variation of $(\alpha h\nu)^2$ with photon energy ($h\nu$) allow to establish the band gap of samples which is important for photocatalytic processes [40]. The band gap value increases slightly from 3.09 for TiO_2 to 3.18 and 3.19 eV for PEI and DT-TiO_2, respectively (Table 1).

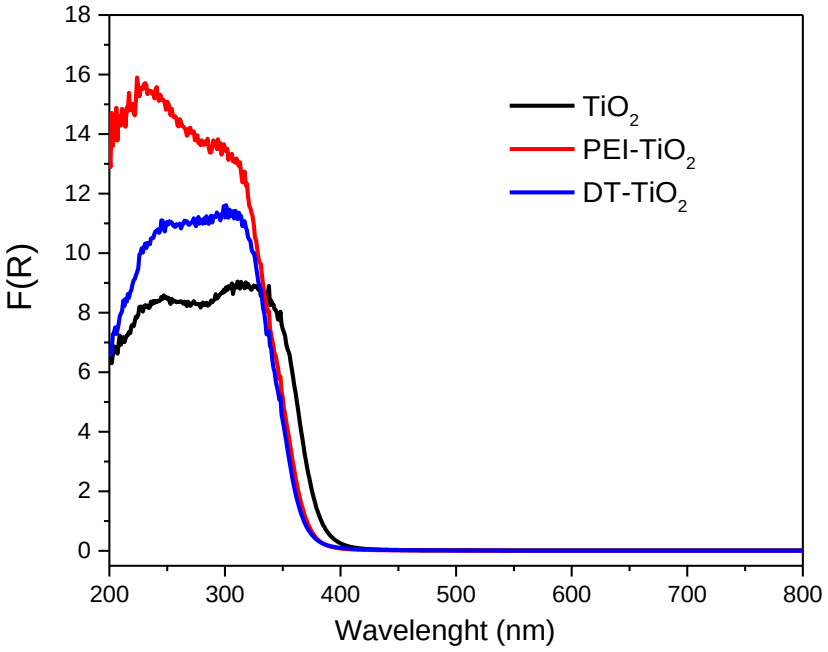

Fig. 6. DRUV-Vis spectra of TiO_2 and functionalized samples.

Figure 7 shows the fluorescence spectra of synthesized TiO_2 and PEI-TiO_2 materials. The PL spectrum of commercial P25 Degussa TiO_2 has also been added to the plot to compare and the results were recorded with the excitation wavelength, 250 nm. The existence of an intense peak around 400 nm is related with the band gap transition of TiO_2 and it is present in all samples. Other peaks in the long wavelength range of 450-475 nm are attributed to the defects/vacancies of oxygen on surface. The PL spectra can be related to the recombination process of the electron-hole pair at the surface [41]. A clear reduction in photoluminescence intensity was observed in synthesized TiO_2 and modified PEI-TiO_2 in comparison with commercial TiO_2. Indeed, a higher reduction was detected in the presence of PEI polymer anchored to TiO_2 surface, which is the incorporation of polymer quench more than 50 % of the fluorescence of TiO_2. That means PEI-TiO_2 catalyst has a smaller recombination rate and more efficient separation of electron-hole pair compared with bare TiO_2 catalysts [42].

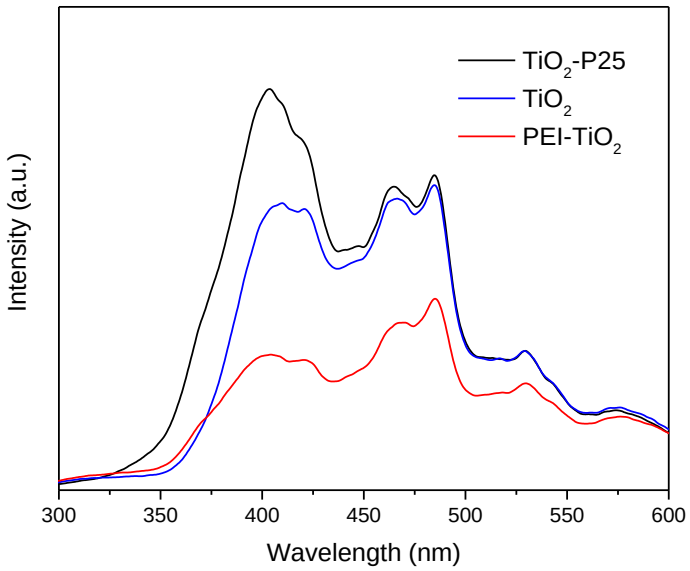

Fig. 7. PL spectra of TiO_2, PEI-TiO_2 and commercial P25 TiO_2.

To conclude the characterization of our materials, we have also investigated the electrochemical properties of TiO_2, PEI-TiO_2 and DT-TiO_2 modified carbon paste electrodes (MCPE) in buffered (pH = 7.4) and acid aqueous systems using cyclic voltammetry (CV). Fig. 88 displays cyclic voltammograms (scan rate 50 and 100 mV/s) for electrode modified with TiO_2 nanoparticles in 0.5 M PBS (pH = 7.0). As can be observed, the cathodic current follows an exponentially rising behavior, but a cathodic peak is not observed even scanning further progressively in the negative direction. However, after returning the potential a clear anodic peak is obtained. This process has been discussed in the literature in relation to films made of sintered TiO_2 nanoparticles, where the electrolyte can penetrate the layer and is related to the reversible conduction band filling [43]. By changing the scan rate, the current intensity of the anodic peak, associated to the oxidation of TiO_2(III) species formed after titanium oxide nanoparticles reduction, increases but the shape is the same as that in the previous case. The negative charge accumulated is compensated by the adsorption of protons or cations from the electrolyte according to the following reaction: $Ti(IV)(TiO_2) + e^- + H^+$ or $M^+(aq) \rightarrow Ti(III)(TiO_2) + H^+$ or $M^+(TiO_2)$. The good linearity of anodic peaks with the increasing scan speed reveals that the K^+ electrolyte cation insertion into the sample corresponds to a semi diffusion-controlled process and hence the system can be treated as quasi-reversible which is consistent with the presence of reversible surface states. In various aqueous redox systems, the CV peaks are generally related to the concentration of H^+ ions, and the effect of pH is consistent with a single electron–single proton reduction process [44]. Cyclic voltammetry experiments performed in aqueous 0.1 M $NaClO_4$ / 1 mM $HClO_4$ demonstrates the involvement of protons in the reduction-oxidation process. A similar voltammetric response is obtained and no cathodic peaks are clearly observed. However, when the potential is scanned into more negative values, two oxidation peaks occur at -0.80 V and -0.23 V,

respectively. As suggested by Marker and co-workers proton adsorption may occur in the vicinity of two distinct binding Ti(III)(TiO_2) sites giving rise to two different reduction-oxidation processes [45].

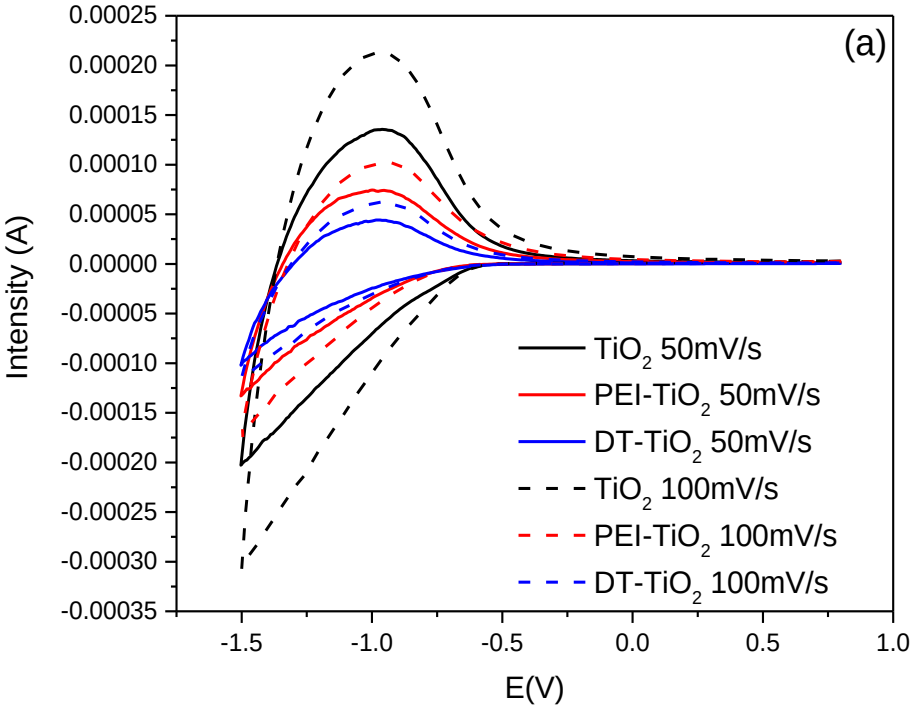

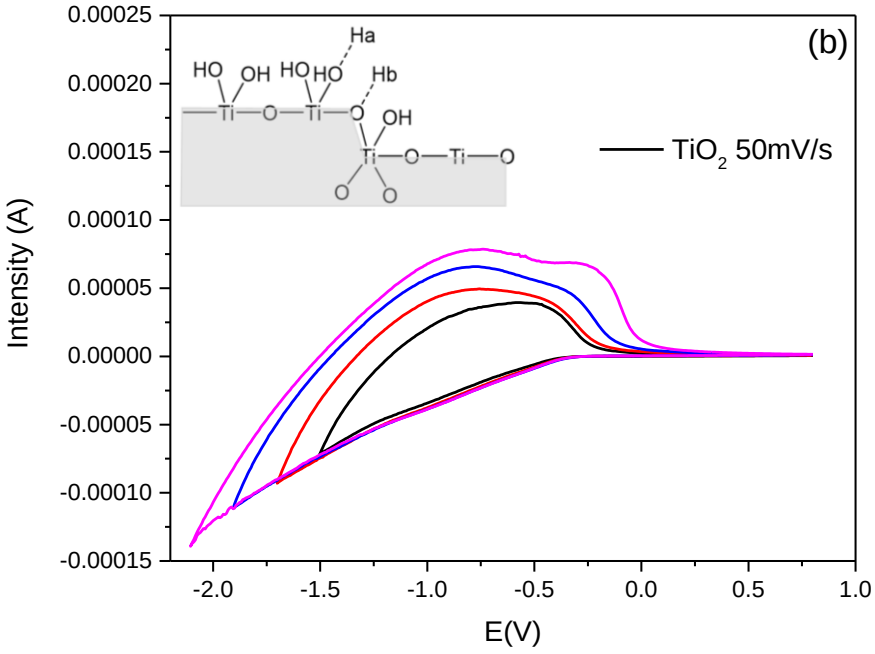

Fig. 8. Cyclic voltammograms obtained for MCPE (a) with TiO_2, PEI-TiO_2 and DT-TiO_2 nanoparticles immersed in aqueous 0.1 M phosphate buffer pH 7 with a reversal potential V_f =

-1.5 V (scan rate 50 and 100 mV/s) (b) with TiO_2 nanoparticles immersed in aqueous 0.1 M $NaClO_4$/1 mM $HClO_4$ with variable reversal potential (scan rate 50 mV/s) vs Ag/AgCl(s) KCl(3M) as reference electrode.

After surface functionalization of TiO_2 by two different approaches, CV of PEI-TiO_2 and DT-TiO_2 have also been recorded in phosphate buffered solution (PBS pH = 7.4). As can be seen in Fig. 88 (a), under similar experimental conditions, the CV for PEI-TiO_2, synthesized by surface-grown polymerization of polyethylenimine onto TiO_2 surface, shows a decrease of the current associated to the anodic peak in comparison to the anodic peak of the pristine TiO_2 nanoparticles. Similarly, the CV recorded for DT-TiO_2 shows an important decrease of the anodic current in comparison to not just pristine TiO_2 but also in comparison to the former functionalized material PEI-TiO_2. These results, obtained scanning at similar scan speed, suggest a decrease in the size of the diffusion layer and hence the existence of a diffusion limited redox process by the adsorption of the cation from the electrolyte onto the surface of TiO_2. In PEI-TiO_2 and DT-TiO_2 the nanoparticle inner mesopores are fully occupied as the BET studies indicate, but the decrease of surface area observed is higher in DT-TiO_2 synthesized by a classical post synthetic silanization procedure, so it can be concluded than the diffusion process of the cation from the electrolyte to counter balance the accumulated charge on the TiO_2 surface is highly influenced by the type of ligand and hence the functionalization procedure performed in this work.

To explore the influence of amino ligands attached to the TiO_2 surface CV experiments were realized in buffered (0.1 M $NaClO_4$/1 mM $HClO_4$) aqueous solutions as electrolyte. Fig. 9 shows a similar response to that previously observed for bare TiO_2 NPs when scanning towards negative potentials with the absence of a clear cathodic peak; nevertheless, after reversal of the scan direction two peak features are observed during oxidation at -1.0 and -0.33 V, being this second peak more pronounced when the scanning reversal potential reach more negative values (V_f = from -1.5 to -2.1 V). Previous reports about branched polyethyleneimine cyclic voltammetry studies show the presence of a pronounced broad peak at more positive potentials, -0.33 V, can be tentatively attributed to the oxidation of terminal NH_2 groups of hyperbranched PEI polymer [46].

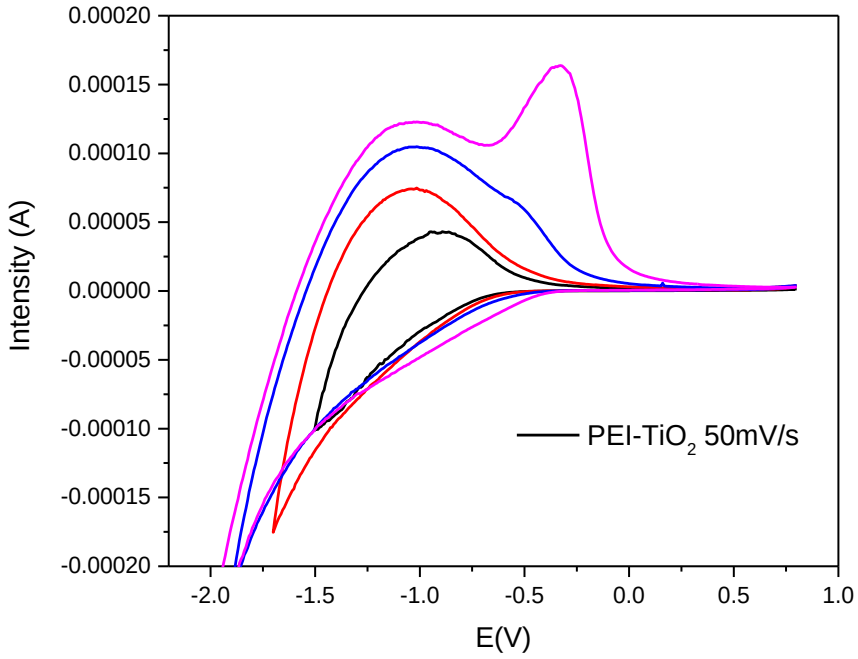

Fig. 9. Cyclic voltammograms obtained for MCPE with PEI-TiO_2 immersed in aqueous in aqueous 0.1 M $NaClO_4$/1 mM $HClO_4$ with a reversal potential V_f = -2.0 V against Ag/AgCl(s) KCl(3M) as reference electrode (scan rate 50 mV/s).

4.2. Photocatalytic degradation of aqueous Methylene Blue (MB)

The relatively low calcination temperature used in this work, 400 °C, allows obtaining TiO_2 NPs, with high specific surface area and narrow pore size distribution, containing anatase and brookite phases. All of them, properties that explain their high photocatalytic activity and efficiency for the degradation of many organic contaminants like methylene blue (MB) [47, 48], chosen as pollutant model molecule in this work. The photocatalytic degradation of MB was performed under UV irradiation (365 nm) and 36 W using catalyst load of 0.4 g L^{-1}. The zeta potential was calculated before and after treatment of the TiO_2 samples in aqueous phosphate buffer solution (pH 7.4) after 1 and 24 h (Table *2*). The zeta potential of pure TiO_2 nanoparticles varied slightly from -26.88 to -31.95 with time, which is consistent with the deprotonation of Ti-O-H groups under these slightly basic conditions and hence the particle surface is negatively charged (isoelectric point for TiO_2 anatase surfaces is expected to be IEP = 6.1) [49]. The presence of PEI and DT induces the zeta potential of TiO_2 nanoparticles shifting from -31.95 to higher -5.5 and -17.67, for PEI and DT-TiO_2, respectively, indicating the existence of negative charge on the titanium oxide surface even after functionalization. These results support the good dispersion of functionalized nanoparticles in aqueous media based on the existence of repulsive interactions and simultaneously explain the efficiency of this materials as adsorbents of positive charged molecules as methylene blue. The degradation percentage using

DT and PEI-TiO_2 as catalysts (55 and 54% in 60 min) was higher than the obtained for TiO_2 (35.6% in 60 min). After 120 min, 81.5 and 97.4% of MB was degraded by DT and PEI-TiO_2, instead of the 72.5% degradation value obtained with bare TiO_2 NPs (Table 2). Similar percentage of degradation of MB was found by Ahmed and coworkers [41] with Ag nanoparticles on titania surface using high catalyst load of 1 g L^{-1} and under high pressure mercury lump.

As can be seen in Fig. 10, the graphical representation of $\ln(C/C_o)$ *vs* reaction time shows a good linear correlation between them meaning that the degradation of MB is a first-order reaction. The calculated value of *k* (reaction rate constant, min^{-1}) is higher for PEI-TiO_2 ($1.8 \cdot 10^{-2}$ min^{-1}) than for DT-TiO_2 ($1.4 \cdot 10^{-2}$ min^{-1}) and nearly doubles the *k* values calculated for unmodified TiO_2 ($1.0 \cdot 10^{-2}$ min^{-1}) (Table *2*). The photocatalytic activity of PEI-TiO_2 recovered material was tested in the degradation of MB under similar conditions. The reused PEI-TiO_2 (PEI-TiO_2-R) retains its activity after the first run. The stability of the polymer on the surface of TiO_2 was confirmed by FTIR analysis (Fig. S5). The bands associated with hyperbranched PEI polymer still appear indicating that the material is fairly stable under photocatalytic conditions.

Table 2. Photocatalytic degradation of MB using TiO_2 samples[a]

Catalyst	*k* (min^{-1})[b]	Degradation at 60 min (%)	Degradation at 120 min (%)	Zeta potential after 1 h (mV)[c]	Zeta potential after 24 h (mV)[c]	Adsorption of MB (%)[d]
TiO_2	$1.0 \cdot 10^{-2}$	35.6	72.5	-26.88	-31.95	5
DT-TiO_2	$1.4 \cdot 10^{-2}$	55.3	81.5	-	-17.67	5
PEI-TiO_2	$1.8 \cdot 10^{-2}$	54.3	97.4	-11.03	-5.28	5
PEI-TiO_2-R[e]	$1.6 \cdot 10^{-2}$	43.3	84.7	-	-	3

[a] Reaction conditions: 20 mg of catalyst, 50 mL of solution of 0.04 mM MB solution, UV irradiation at 365 nm and 36 W.
[b] Reaction rate constant (*k*) calculated by graphical representation of $\ln(C/C_o)$ vs reaction time.
[c] Calculated after treatment of the TiO_2 samples in aqueous phosphate buffer pH 7.4.
[d] Calculated by recovered UV-vis spectra of MB in presence of TiO_2 and under conditions of darkness.
[e] Reused PEI-TiO_2 material (first run).

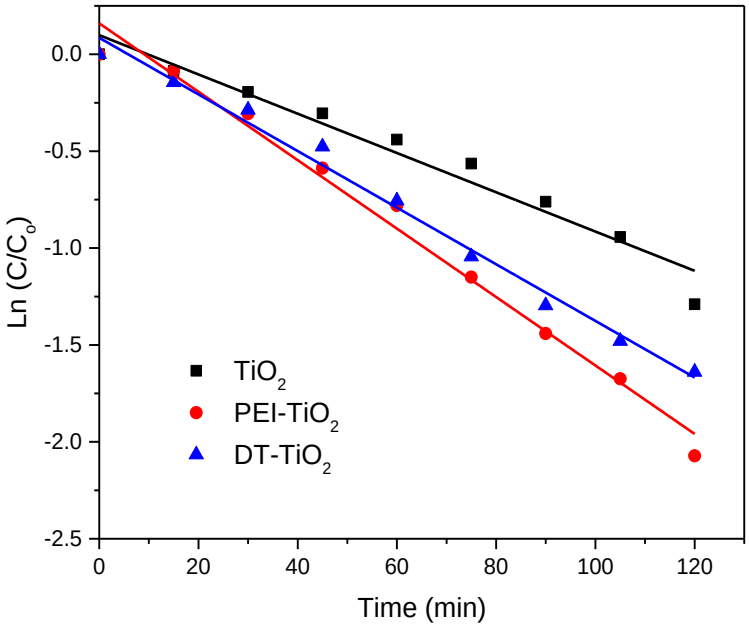

Fig. 10. Photocatalytic degradation of MB using TiO_2 samples

To recognize the primary reactive species involved in the degradation of methylene blue over TiO_2 nanoparticles under UV light irradiation, we used different radical scavengers in a concentration of 2 mM. Thus, tert-butanol (t-BuOH), benzoquinone (BQ) and ascorbic acid (AA) were utilized to scavenge hydroxyl free radicals (·OH), superoxide free radicals ($\cdot O_2^-$) and positive holes (h^+), respectively [23, 42]. As shown in Fig. S6, the photodegradation percentage of MB was reduced with the addition of the different scavengers, especially with ascorbic acid, indicating that photogenerated positive holes are the primary reactive species for MB degradation. Superoxide free radicals are also involved in the process due to the similar scavenged effect with the addition of benzoquinone to the reaction. Nevertheless, hydroxyl free radicals are not the main reactive species (but are also important) for degradation of MB, since the t-BuOH scavenger exhibits a lower influence on the percentage of degradation. The effect of the Ascorbic acid scavenger is more pronounced on the PEI-TiO_2 degradation reaction since the percentage decrease from 97 % to 43 %. This fact displays that in the reaction (without scavenger) a larger number of positive holes exists, which assists and promotes the degradation in a greater way than the reaction with bare TiO_2, and also improves the electron-hole recombination. On the other hand, the highest reduction produced on the degradation percentage with TiO_2 when benzoquinone is used indicates that superoxide radicals show more influence in MB degradation on pure titania surface. With the UV light irradiation, the electron leaves the conduction band and a positive hole is generated in the valence band [13, 50]. The mechanism for the degradation of MB with synthesized TiO_2 is the same that previously described under UV irradiation [13], as shown in Scheme 2.

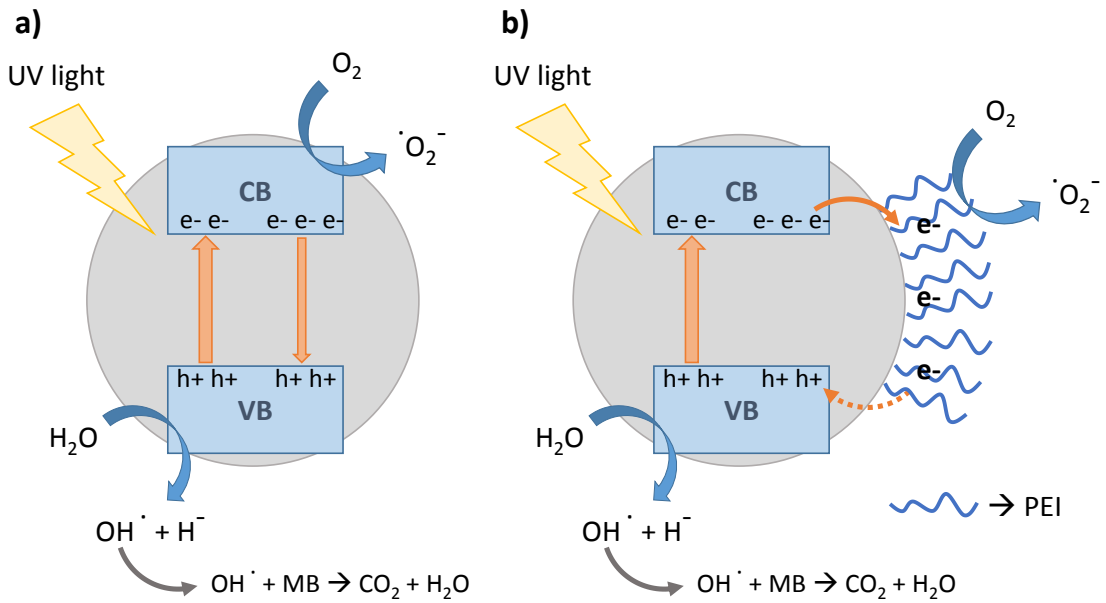

Scheme 2. Proposed mechanism of degradation of MB with a) TiO_2 and b) PEI-TiO_2.

However, the proposed mechanism for the PEI-TiO_2 material has a slight modification (Scheme 2). Polyethylenimine has been previously shown as effective low-work function modifier for organic devices, like solar cells [51], due to its ability to reduce the work function of TiO_2 films from 4.42 eV to 4.20 eV in PEI-TiO_2 [25]. Thus, the PEI network could receive the photogenerated electrons from conduction band of TiO_2 and then these electrons can react with the oxygen molecule to generate superoxide free radicals. The photogenerated positive holes in the valence band can oxidize water molecules to produce hydroxyl radicals. These radicals are usually reacting with methylene blue molecules, which finally transform into CO_2 + H_2O. The electron-rich nitrogen atoms in polymer PEI could fill the photogenerated positive holes, reducing the electron-hole recombination from CB and improving electron mobility in the system [52]. This proposed mechanism is supported by the PL results (Fig. 7), where the decrease in PL intensity for the PEI-TiO_2 sample indicated transfer of photogenerated electrons from TiO_2 to PEI polymer, thus reducing the electron-hole recombination probability.

4.3. Catalytic tests

The versatility of the materials synthesized in this work is reflected in their applications as basic catalysts for several multicondensation reactions. It is well known the application of organosilica materials as heterogeneous catalysts due not only to the unique properties of the siloxane framework but also to the nature of the chemical functionality attached to the support. Since silica surface owns silanol groups with acidic properties (isoelectronic point of silica goes from 1.5 to 3.5) electrophilic activation of carbonyl or nitroalkene groups takes place through the formation of

hydrogen bond (Si-O-H…O=C) which enhance their reactivity towards nucleophiles. In the case of heterogeneous catalyst based on silica functionalized with basic groups the role of the acidic surface silanol groups is not fully explained in reactions of the type of Knoevenagel condensation or aldol reactions. Some authors conclude that basic groups interact with surface silanol groups decreasing their basic strength [53]. On the contrary, other authors propose that silanol groups influence greatly the mechanism by transferring a proton to enhance cooperative ion-pair mechanism, in the presence of basic functionalities as tertiary or secondary amines [54], or to support the creation of an imine intermediate in case of primary amines [55, 56]. Lately, Thybaut and coworkers have demonstrated the benefit of water in the recyclability of amino functionalized mesoporous silica in aldol reaction since water increases the hydration rate of iminium intermediates and improve the stability of the catalyst. Furthermore, the deactivation of the catalyst can also be avoided by increasing the hydrophobicity of the silica surface by end capping the surface silanol groups [57]. Niobium containing materials based on SBA-15 with nitrogen-containing organic modifier were prepared by Calvino-Casilda [26], these materials, which exhibit acid and basic sites promote greatly the Knoevenagel condensation via the ion-pair mechanism.

Bearing in mind all these proposals we performed several catalytic studies by using PEI-TiO_2 and DT-TiO_2 materials since they fulfil some of the requirements previously described. Both materials possess high loading basic groups (primary and secondary amines) and PEI-TiO_2 also presents tertiary amines. Simultaneously, they possess Ti-O-H surface groups much less acidic (IEP = 6.1) than silanol groups which may still act as mild acid groups to become these catalysts bifunctional ones. The presence of acid Lewis Ti^{4+} center may enhance the synergies between the Ti–O(H)…Ti^{4+} and amine groups in close proximity. These acid Lewis centres are not strong enough to break apart the basic sites attached on the surface but may act as acids in reactions rather than simply stabilizing the transitions states formed with hydrogen. This improvement has been previously observed in nitroaldol reaction with amino propyl groups anchored onto Al-MCM-41 by establishing comparable Si–O(H)…Al^{3+} interactions [58].

4.3.1. Knoevenagel condensation reaction

In order to test the properties of these materials as catalysts, the Knoevenagel condensation between benzaldehyde and malononitrile or ethyl cyanoacetate was performed (Table 3 and Fig. S7) with functionalized TiO_2 NPs as catalysts and bare TiO_2 as blank, obtaining a negligible activity with this last. The catalytic system PEI-TiO_2 is excellent in malononitrile condensation with ethanol as solvent and at room temperature, obtaining 98% yield after 15 min of reaction time (Entry 1) and 99% yield in 30 min (Entry 2). When ethyl cyanoacetate was used different reaction conditions were evaluated (Entries 3-13). The best result, 97% conversion, was obtained in 2 h of reaction and at 80 ^{o}C using, as well, ethanol as solvent. This value decreases at 77% when temperature decreases to 60 ^{o}C. A similar conversion, 77%, is obtained without

solvent at 80 ^{o}C. The influence of solvent was studied by using PEG/H_2O, dichloromethane and toluene. Thus, when polar solvents were used higher conversion values were obtained in comparison with toluene. The reaction was tested, as well, in water and in the absence of solvent, obtaining a lower conversion in aqueous media 55%, but an interesting 71% conversion value solvent-less condition at 60 ^{o}C. With DT-TiO_2 catalyst (Entries 14-17), the activity decreases significantly, since the nitrogen loading value is half of the nitrogen content of PEI-TiO_2, this behaviour is expected. Nevertheless, the effect of solvent in the catalytic reaction is the same, so we hypothesized similar reaction mechanism for both materials tested in this work.

As previously mentioned, two possible mechanism are fully accepted in literature, named as the imine intermediate and the ion-pair mechanisms. The former is usually proposed for primary amines functionalized materials, with secondary and tertiary amines enable to form imine intermediates the latter is accepted. The effect of solvent in both mechanisms displays opposing trends. In those reactions which proceed through an ion par mechanism the activity improves with increasing solvent polarity. On the contrary, non-polar solvents seems to facilitate the imine intermediate formation in primary amine heterogeneous catalysts by concentrating the reactants at the catalyst surface. In this work, the best conversion values are obtained in polar solvents. Since the hyperbranched PEI polymer contains approximately 30% of primary amines ($pK_a \approx 9.4$), 40% of secondary amines ($pK_a \approx 8.6$-4.4 dependent on other nearby amino groups) and 30% of tertiary amines (being significantly basic to be protonated above pH 0) [59, 60], we propose the existence of an ion-pair mechanism where the carbanion intermediate, formed by the abstraction of methylene proton in ethyl cyanoacetate by the nitrogen basic atom, reaches a major stabilization in polar solvents as ethanol and dichloromethane. Anyway, the formation of an imine intermediate in the case of less abundant primary amino groups cannot be discarded in PEI and DT-TiO_2 materials. It could be accepted that due to the lower number of primary NH_2 groups, their impact on the global ion pair mechanism is negligible or that the imine formation mechanism is also favored in polar media. The first hypothesis is supported by the lower conversion values obtained with DT-TiO_2 where the nitrogen loading decreases significantly but also the amount of primary amino groups increases which makes impossible to understate their negative influence in the ion pair mechanism in polar solvents. The second hypothesis can be supported by the data previously reported with amino functionalized silsesquioxane compounds, with these catalysts the influence of the solvents follows the opposite tendency to that expected, the activity increases also in polar solvents [61]. Sangs et al [61] explained this solvent effect due to the higher hydrophobicity of silsesquioxane in comparison to silica surface and their partitioning effect. Similarly, the efficient functionalization of the TiO_2 surface with the hyperbranched polymer in PEI-TiO_2 would increase their hydrophobic character of the TiO_2 surface and consequently, would not concentrate polar reactants near the catalyst surface.

1 Table 3. Knoevenagel condensation reaction catalysed by titanium dioxide catalysts[a]

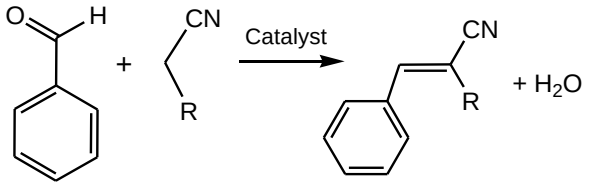

R = CN (Malononitrile)
R = CO_2Et (Ethyl cyanoacetate)

Entry	Catalyst	Substrate	T (^oC)	Time (h)	Solvent	Conversion (%)[b]	Yield (%)[c]
1	PEI-TiO_2	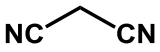	25	15	EtOH	94.2	98
2	PEI-TiO_2		25	30	EtOH	99	99
3	PEI-TiO_2	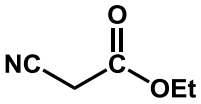	25	8	EtOH	44.7	
4	PEI-TiO_2		25	24	EtOH	70.4	
5	PEI-TiO_2		60	2	EtOH	77.3	75
6	PEI-TiO_2		60	3	EtOH	85.6	
7	PEI-TiO_2		60	2	CH_2Cl_2	53.2	
8	PEI-TiO_2		60	2	PEG/H_2O (1:1 vol)	60.0	
9	PEI-TiO_2		60	2	Toluene	12.0	
10	PEI-TiO_2		60	2	H_2O	55.1	
11	PEI-TiO_2		60	2	Solvent less	71.1	
12	PEI-TiO_2		80	2	EtOH	97.2	95
13	PEI-TiO_2		80	2	Solventless	77.7	
14	DT-TiO_2	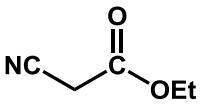	60	120	EtOH	60.6	
15	DT-TiO_2		60	120	Solvent less	47.7	

16	DT-TiO_2	60	120	H_2O	49.5
17	DT-TiO_2	60	120	Toluene	7.9

[a] Reaction conditions: 50 mg of catalyst, 5 mL of solvent, 11 mmol of benzaldehyde, 11 mmol of malononitrile or ethyl cyanoacetate

[b] Conversions are based on benzaldehyde (Determined by GC)

[c] Yield of the isolated product identified by NMR spectroscopy.

4.3.2. One pot condensation reaction

The catalytic activity of these materials was also tested for multicondensation reaction to obtain 2-amino-chromene derivatives. The results are reported in Table 4 (See also Figs. S8-S9). When malonotrile (pK_a = 11.1) was used the reaction was quantitative for PEI-TiO_2 after two hour's reaction time at room temperature (Entry 19). DT-TiO_2, as expected, produces lower yields (Entry 20). The compound 2,2'-(phenylmethylene)bis(3-hydroxy-5,5-dimethylcyclohex-2-en-1-one) was obtained using ethyl cyanoacetate (pK_a = 13.1) (Entry 21). The condensation of benzaldehyde and dimedone takes place preferentially due to the higher acidity of dimedona (pK_a = 12).

Table 4. Multicondensation reaction catalysed by functionalized TiO_2 samples[a]

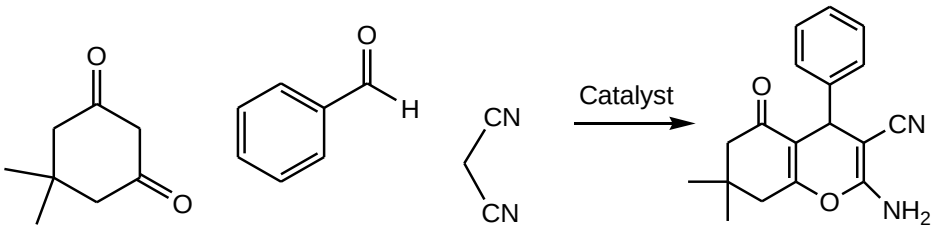

Entry	Catalyst	T (^oC)	Time (min)	Solvent	Yield (%)[b]
18	PEI-TiO_2	25	30	EtOH	85
19	PEI-TiO_2	25	120	EtOH	100
20	DT-TiO_2	25	120	EtOH	85

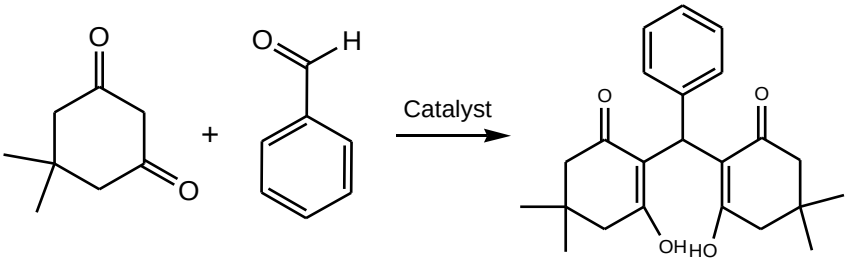

Entry	Catalyst	T (^{o}C)	Time (min)	Solvent	Yield (%)[b]
21	PEI-TiO_2	60	120	EtOH	98

[a] Reaction conditions: 25 mg of catalyst, 5 mL of ethanol, 5.5 mmol of benzaldehyde, malononitrile and 5,5-dimethylcyclohexane-1,3-dione

[b] Yield of the isolated product identified by ^{1}H NMR spectroscopy.

4.3.3. Biginelli reaction

Finally, the Biginelli reaction has been also tested using PEI-TiO_2 as catalyst. This reaction involves one-pot synthesis of 3,4-dihydropyrimidin-2(1H)-ones using benzaldehyde, ethyl acetoacetate as active methylene compound and urea or thiourea. As can be seen in Table 5, entries 22 and 23 (Fig. S10), the yields obtained are 71.7% using ethanol as solvent and 66% under solvent less conditions. These results are comparable to those obtained with other organocatalysts based on tethered imidazolium ionic liquid onto mesoporous SBA-15 material but they carried out the reaction with 40 mL of glacial acetic acid and at 100 ^{o}C for 3 h [62]. When the reaction proceeded with thiourea, the product was obtained in 73.5% of yield (Entry 24 and Fig. S11). Jing and coworkers used ZrO_2-Al_2O_3-Fe_3O_4 as catalyst which showed lower yield (63.4%) that obtained in this work, under more severe conditions (140 ^{o}C for 5 h) [63]. With the aim to prove the stability of PEI polymer under the hardest reaction conditions, like in Biginelli reaction, ^{1}H NMR spectra were recorded to commercial PEI before and after to be subjected at 80 ^{o}C during 2 h. The results in Fig. S12 show no significant change on the signals corresponding to methylene and amino groups [60].

Table 5. Biginelli condensation reaction catalysed by titanium dioxide catalysts[a]

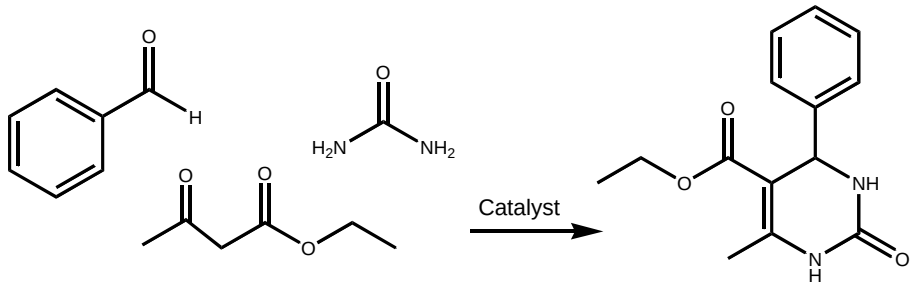

Entry	Catalyst	T (^{o}C)	Time (min)	Solvent	Yield (%)[b]
22	PEI-TiO_2	80	120	EtOH	72
23	PEI-TiO_2	80	120	Solvent less[c]	66

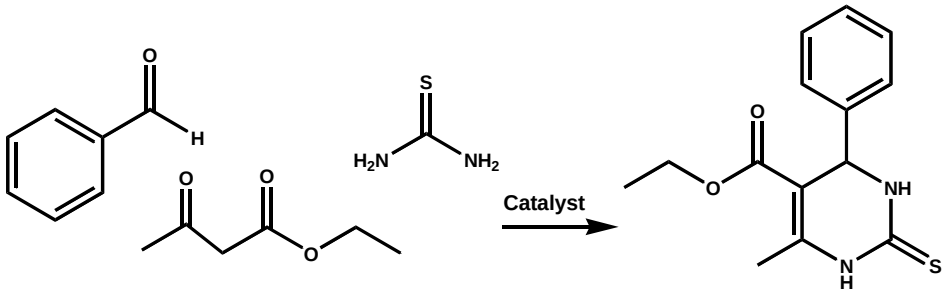

Entry	Catalyst	T (^{o}C)	Time (min)	Solvent	Yield (%)[b]
24	PEI-TiO_2	80	120	EtOH	74
25	PEI-TiO_2	80	120	Solvent less[c]	54

[a] Reaction conditions: catalyst: 50 mg, solvent: 2 mL of ethanol, substrate: 1 mmol

[b] Yield of the isolated product identified by NMR spectroscopy.

[c] Reaction conditions: Catalyst: 25 mg, substrate: 2 mmol

As representative examples, PEI-TiO_2 catalyst was recovered and recycled for several Knoevenagel condensations. In both condensations, PEI-TiO_2 catalyst was easily recovered by centrifugation. The results for five consecutive catalytic runs are shown in Fig. 11 and Fig. 12712. Conversion and selectivity values are retained for Knoevenagel condensation of benzaldehyde and malononitrile. In the case of Knoevenagel condensation of benzaldehyde with ethyl cyanoacetate a slight decrease in conversion is observed. However, we have studied recovered PEI-TiO_2, after

photocatalytic and catalytic reactions, by FTIR spectroscopy establishing that the PEI polymer is still anchored to the TiO_2 surface indicating that the material is fairly stable under catalytic conditions (Fig S5).

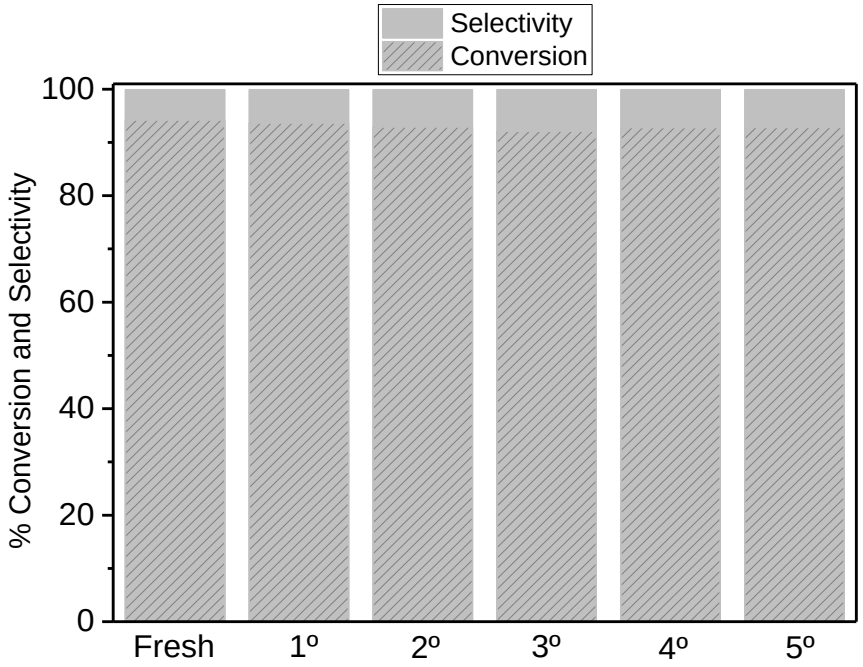

Fig. 11. Catalytic activity of PEI-TiO_2 for Knoevenagel condensation of benzaldehyde with malononitrile in 5 consecutive reaction cycles.

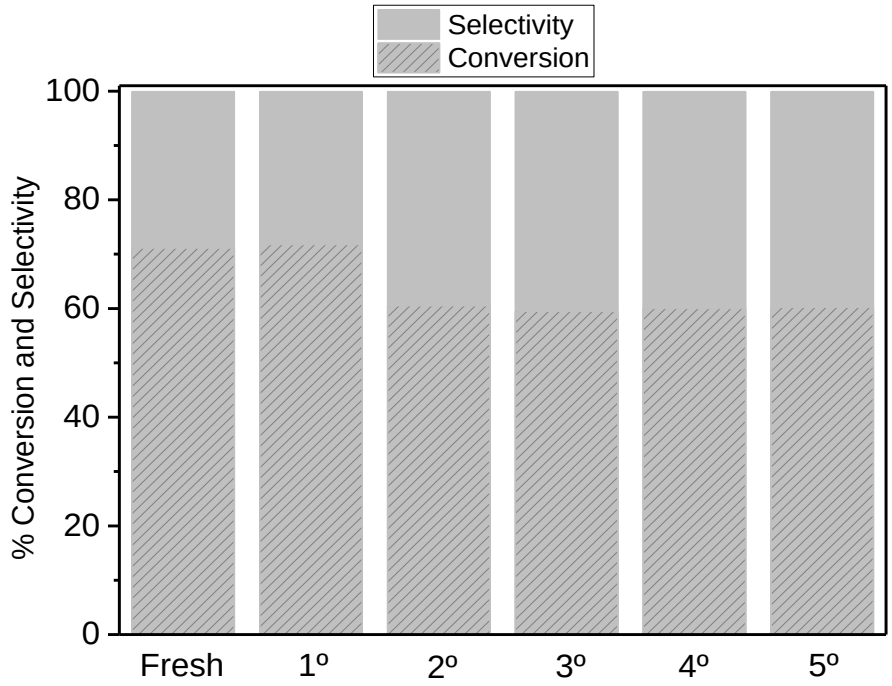

Fig. 127. Catalytic activity of PEI-TiO_2 for Knoevenagel condensation of benzaldehyde with ethyl cyanoacetate in 5 consecutive reaction cycles.

5. Conclusions.

Crystalline TiO_2 nanoparticles have been prepared by a sol-gel procedure with a certain ratio of brookite phase due to the low calcination temperature used during the synthesis. The post functionalization of TiO_2 NPs by Ti-O-C bond formation with hyperbranched polyethylenimine polymer PEI or by Ti-O-Si bond formation with N^1-(3-trimethoxysilylpropyl)diethylenetriamine has been successfully achieved. The fully characterization of both materials allow us to correlate their excellent activity as photocatalyst in the degradation of MB or as basic catalysts in C-C bond reactions formation with their chemical structure and the own features of the materials. The PEI functionalized TiO_2 material shows higher activity for photodegradation of MB and Knoevenagel condensation reactions than the DT-TiO_2 material functionalized with a commercially available ligand. In addition, the separation and recovery of PEI-TiO_2 NPs make it reusable for several times as catalyst without loss of activity.

6. Acknowledgements

We gratefully acknowledge financial support from the MICINN (project CTQ2015-66164-R and RTI2018-094322-B-I00).

References

[1] K. Brown, T. Thurn, L. Xin, W. Liu, R. Bazak, S. Chen, B. Lai, S. Vogt, C. Jacobsen, T. Paunesku, G.E. Woloschak, Intracellular in situ labeling of TiO_2 nanoparticles for fluorescence microscopy detection, Nano Research 11 (2018) 464-476. https://doi.org/10.1007/s12274-017-1654-8.

[2] K.T. Thurn, H. Arora, T. Paunesku, A. Wu, E.M.B. Brown, C. Doty, J. Kremer, G. Woloschak, Endocytosis of titanium dioxide nanoparticles in prostate cancer PC-3M cells, Nanomed. Nanotechnol. Biol. Med. 7 (2011) 123-130. https://doi.org/10.1016/j.nano.2010.09.004.

[3] G.K. Mor, K. Shankar, M. Paulose, O.K. Varghese, C.A. Grimes, Use of Highly-Ordered TiO_2 Nanotube Arrays in Dye-Sensitized Solar Cells, Nano Lett. 6 (2006) 215-218. https://doi.org/10.1021/nl052099j.

[4] A. Ziarati, A. Badiei, R. Grillo, T. Burgi, 3D Yolk@Shell TiO_2–x/LDH Architecture: Tailored Structure for Visible Light CO_2 Conversion, ACS Appl. Mater. Interfaces 11 (2019) 5903-5910. https://doi.org/10.1021/acsami.8b17232.

[5] K.-Q. Lu, X. Xin, N. Zhang, Z.-R. Tang, Y.-J. Xu, Photoredox catalysis over graphene aerogel-supported composites, J. Mater. Chem. A 6 (2018) 4590-4604. http://dx.doi.org/10.1039/C8TA00728D.

[6] B. Weng, K.-Q. Lu, Z. Tang, H.M. Chen, Y.-J. Xu, Stabilizing ultrasmall Au clusters for enhanced photoredox catalysis, Nat. Commun 9 (2018) 1543. https://doi.org/10.1038/s41467-018-04020-2.

[7] X. Zhao, Y. Zhang, P. Wen, G. Xu, D. Ma, P. Qiu, NH2-MIL-125(Ti)/TiO_2 composites as superior visible-light photocatalysts for selective oxidation of cyclohexane, Molecular Catalysis 452 (2018) 175-183. https://doi.org/10.1016/j.mcat.2018.04.004.

[8] A. Ziarati, A. Badiei, R. Luque, Black hollow TiO_2 nanocubes: Advanced nanoarchitectures for efficient visible light photocatalytic applications, Appl. Catal. B 238 (2018) 177-183. https://doi.org/10.1016/j.apcatb.2018.07.020.

[9] C. Han, S.-H. Li, Z.-R. Tang, Y.-J. Xu, Tunable plasmonic core–shell heterostructure design for broadband light driven catalysis, Chem Sci 9 (2018) 8914-8922. http://dx.doi.org/10.1039/C8SC04479A.

[10] Y. Liang, K. Su, L. Cao, Z. Li, Lithium doped TiO_2 as catalysts for the transesterification of bisphenol-A with dimethyl carbonate, Molecular Catalysis 465 (2019) 16-23. https://doi.org/10.1016/j.mcat.2018.12.022.

[11] S. Bak, S.M. Lee, H.M. Hwang, H. Lee, Phase-selective modulation of TiO_2 for visible light-driven CH arylation: Tuning of absorption and adsorptivity, Molecular Catalysis 471 (2019) 71-76. https://doi.org/10.1016/j.mcat.2019.04.017.

[12] S. Sánchez-Muñoz, D. Pérez-Quintanilla, S. Gómez-Ruiz, Synthesis and photocatalytic applications of nano-sized zinc-doped mesoporous titanium oxide, Mater. Res. Bull. 48 (2013) 250-255. https://doi.org/10.1016/j.materresbull.2012.10.032.

[13] S.G. Kumar, L.G. Devi, Review on Modified TiO_2 Photocatalysis under UV/Visible Light: Selected Results and Related Mechanisms on Interfacial Charge Carrier Transfer Dynamics, J. Phys. Chem. A 115 (2011) 13211-13241. https://doi.org/10.1021/jp204364a.

[14] C. McManamon, J. O'Connell, P. Delaney, S. Rasappa, J.D. Holmes, M.A. Morris, A facile route to synthesis of S-doped TiO_2 nanoparticles for photocatalytic activity, J. Mol. Catal. A: Chem. 406 (2015) 51-57. https://doi.org/10.1016/j.molcata.2015.05.002.

[15] A. Didi, L.M. Gómez-Calcerrada, A. Benhamou, S. Gómez-Ruiz, Versatility in the catalytic and photocatalytic reactions of composites based on Zr- and Zr-Pd-doped titania nanoparticles, Ceram. Int. 44 (2018) 17266-17276. https://doi.org/10.1016/j.ceramint.2018.06.187.

[16] A. Abdelhaleem, W. Chu, X. Liang, Diphenamid degradation via sulfite activation under visible LED using Fe (III) impregnated N-doped TiO_2 photocatalyst, Appl Catal B 244 (2019) 823-835. https://doi.org/10.1016/j.apcatb.2018.11.085.

[17] K.S. Min, R.S. Kumar, J.H. Lee, K.S. Kim, S.G. Lee, Y.-A. Son, Synthesis of new TiO_2/porphyrin-based composites and photocatalytic studies on methylene blue degradation, Dyes Pigm 160 (2019) 37-47. https://doi.org/10.1016/j.dyepig.2018.07.045.
[18] K. Geng, Y. Wu, G. Jiang, K. Liu, L. Jiang, RuC@g-C_3N_4(H+)/TiO_2 visible active photocatalyst: Facile fabrication and Z-scheme carrier transfer mechanism, Molecular Catalysis 458 (2018) 33-42. https://doi.org/10.1016/j.mcat.2018.07.026.
[19] E. Galoppini, Linkers for anchoring sensitizers to semiconductor nanoparticles, Coord. Chem. Rev. 248 (2004) 1283-1297. https://doi.org/10.1016/j.ccr.2004.03.016.
[20] X.W. Li, R.G. Song, Y. Jiang, C. Wang, D. Jiang, Surface modification of TiO_2 nanoparticles and its effect on the properties of fluoropolymer/TiO_2 nanocomposite coatings, Appl. Surf. Sci. 276 (2013) 761-768. https://doi.org/10.1016/j.apsusc.2013.03.167.
[21] P. Weerachawanasak, G.J. Hutchings, J.K. Edwards, S.A. Kondrat, P.J. Miedziak, P. Prasertham, J. Panpranot, Surface functionalized TiO_2 supported Pd catalysts for solvent-free selective oxidation of benzyl alcohol, Catal. Today 250 (2015) 218-225. https://doi.org/10.1016/j.cattod.2014.06.005.
[22] J. Zhao, M. Milanova, M.M.C.G. Warmoeskerken, V. Dutschk, Surface modification of TiO_2 nanoparticles with silane coupling agents, Colloids Surf A Physicochem Eng Asp 413 (2012) 273-279. https://doi.org/10.1016/j.colsurfa.2011.11.033.
[23] A. Ziarati, A. Badiei, R. Luque, Engineered bi-functional hydrophilic/hydrophobic yolk@shell architectures: A rational strategy for non-time dependent ultra selective photocatalytic oxidation, Appl. Catal. B 240 (2019) 72-78. https://doi.org/10.1016/j.apcatb.2018.08.058.
[24] F. Loffredo, I.A. Grimaldi, A. De Girolamo Del Mauro, F. Villani, V. Bizzarro, G. Nenna, R. D'Amato, C. Minarini, Polyethylenimine/N-doped titanium dioxide nanoparticle based inks for ink-jet printing applications, J. Appl. Polym. Sci 122 (2011) 3630-3636. https://doi.org/10.1002/app.34775.
[25] D. Yang, P. Fu, F. Zhang, N. Wang, J. Zhang, C. Li, High efficiency inverted polymer solar cells with room-temperature titanium oxide/polyethylenimine films as electron transport layers, J. Mater. Chem. A 2 (2014) 17281-17285. http://dx.doi.org/10.1039/C4TA03838J.
[26] D. Kryszak, K. Stawicka, M. Trejda, V. Calvino-Casilda, R. Martin-Aranda, M. Ziolek, Development of basicity in mesoporous silicas and metallosilicates, Catal Sci Technol 7 (2017) 5236-5248. http://dx.doi.org/10.1039/C7CY00927E.
[27] G. Zhang, Y. Zhang, J. Yan, R. Chen, S. Wang, Y. Ma, R. Wang, One-Pot Enantioselective Synthesis of Functionalized Pyranocoumarins and 2-Amino-4H-chromenes: Discovery of a Type of Potent Antibacterial Agent, J. Org. Chem 77 (2012) 878-888. https://doi.org/10.1021/jo202020m.
[28] A. Solhy, A. Elmakssoudi, R. Tahir, M. Karkouri, M. Larzek, M. Bousmina, M. Zahouily, Clean chemical synthesis of 2-amino-chromenes in water catalyzed by nanostructured diphosphate $Na_2CaP_2O_7$, Green Chem. 12 (2010) 2261-2267. http://dx.doi.org/10.1039/C0GC00387E.
[29] J.M. Rosenholm, A. Penninkangas, M. Lindén, Amino-functionalization of large-pore mesoscopically ordered silica by a one-step hyperbranching polymerization of a surface-grown polyethyleneimine, Chem. Commun. (2006) 3909-3911. http://dx.doi.org/10.1039/B607886A.
[30] S. Lázaro-Navas, S. Prashar, M. Fajardo, S. Gómez-Ruiz, Visible light-driven photocatalytic degradation of the organic pollutant methylene blue with hybrid palladium–fluorine-doped titanium oxide nanoparticles, J. Nanopart. Res. 17 (2015) 94. https://doi.org/10.1007/s11051-015-2902-z.
[31] W. Lu, M. Ling, M. Jia, P. Huang, C. Li, B. Yan, Facile synthesis and characterization of polyethylenimine-coated Fe_3O_4 superparamagnetic nanoparticles for cancer cell separation, Mol Med Rep 9 (2014) 1080-1084. https://doi.org/10.3892/mmr.2014.1906.

[32] J.-G. Li, T. Ishigaki, X. Sun, Anatase, Brookite, and Rutile Nanocrystals via Redox Reactions under Mild Hydrothermal Conditions: Phase-Selective Synthesis and Physicochemical Properties, J. Phys. Chem. C 111 (2007) 4969-4976. https://doi.org/10.1021/jp0673258.
[33] O. Durupthy, J. Bill, F. Aldinger, Bioinspired Synthesis of Crystalline TiO_2: Effect of Amino Acids on Nanoparticles Structure and Shape, Cryst. Growth Des 7 (2007) 2696-2704. https://doi.org/10.1021/cg060405g.
[34] A. Grosman, C. Ortega, Nature of Capillary Condensation and Evaporation Processes in Ordered Porous Materials, Langmuir 21 (2005) 10515-10521. https://doi.org/10.1021/la051030o.
[35] S.K. Das, M.K. Bhunia, A. Bhaumik, Self-assembled TiO_2 nanoparticles: mesoporosity, optical and catalytic properties, Dalton Trans 39 (2010) 4382-4390. http://dx.doi.org/10.1039/C000317D.
[36] R. Anwander, SOMC@PMS. Surface Organometallic Chemistry at Periodic Mesoporous Silica, Chem. Mater. 13 (2001) 4419-4438. https://doi.org/10.1021/cm0111534.
[37] A.K. Thakur, G.M. Nisola, L.A. Limjuco, K.J. Parohinog, R.E.C. Torrejos, V.K. Shahi, W.-J. Chung, Polyethylenimine-modified mesoporous silica adsorbent for simultaneous removal of Cd(II) and Ni(II) from aqueous solution, J. Ind. Eng. Chem 49 (2017) 133-144. https://doi.org/10.1016/j.jiec.2017.01.019.
[38] M.I. Zaki, M.A. Hasan, F.A. Al-Sagheer, L. Pasupulety, In situ FTIR spectra of pyridine adsorbed on SiO_2–Al_2O_3, TiO_2, ZrO_2 and CeO_2: general considerations for the identification of acid sites on surfaces of finely divided metal oxides, Colloids Surf A Physicochem Eng Asp 190 (2001) 261-274. https://doi.org/10.1016/S0927-7757(01)00690-2.
[39] M. Kassir, T. Roques-Carmes, T. Hamieh, A. Razafitianamaharavo, O. Barres, J. Toufaily, F. Villiéras, Surface modification of TiO_2 nanoparticles with AHAPS aminosilane: distinction between physisorption and chemisorption, Adsorption 19 (2013) 1197-1209. https://doi.org/10.1007/s10450-013-9555-y.
[40] N. Zhang, M.-Q. Yang, S. Liu, Y. Sun, Y.-J. Xu, Waltzing with the Versatile Platform of Graphene to Synthesize Composite Photocatalysts, Chem. Rev. 115 (2015) 10307-10377. https://doi.org/10.1021/acs.chemrev.5b00267.
[41] M.F. Abdel Messih, M.A. Ahmed, A. Soltan, S.S. Anis, Facile approach for homogeneous dispersion of metallic silver nanoparticles on the surface of mesoporous titania for photocatalytic degradation of methylene blue and indigo carmine dyes, J. Photochem. Photobiol A 335 (2017) 40-51. https://doi.org/10.1016/j.jphotochem.2016.11.001.
[42] M.A. Ahmed, Z.M. Abou-Gamra, A.M. Salem, Photocatalytic degradation of methylene blue dye over novel spherical mesoporous Cr_2O_3/TiO_2 nanoparticles prepared by sol-gel using octadecylamine template, J. Environ. Chem. Eng. 5 (2017) 4251-4261. https://doi.org/10.1016/j.jece.2017.08.014.
[43] T. Berger, T. Lana-Villarreal, D. Monllor-Satoca, R. Gómez, Charge transfer reductive doping of nanostructured TiO_2 thin films as a way to improve their photoelectrocatalytic performance, Electrochem. Commun. 8 (2006) 1713-1718. https://doi.org/10.1016/j.elecom.2006.08.006.
[44] F. Fabregat-Santiago, I. Mora-Seró, G. Garcia-Belmonte, J. Bisquert, Cyclic Voltammetry Studies of Nanoporous Semiconductors. Capacitive and Reactive Properties of Nanocrystalline TiO_2 Electrodes in Aqueous Electrolyte, J. Phys. Chem. B 107 (2003) 758-768. https://doi.org/10.1021/jp0265182.
[45] F. Marken, A.S. Bhambra, D.-H. Kim, R.J. Mortimer, S.J. Stott, Electrochemical reactivity of TiO_2 nanoparticles adsorbed onto boron-doped diamond surfaces, Electrochem. Commun. 6 (2004) 1153-1158. https://doi.org/10.1016/j.elecom.2004.09.006.
[46] A. Adenier, M.M. Chehimi, I. Gallardo, J. Pinson, N. Vilà, Electrochemical Oxidation of Aliphatic Amines and Their Attachment to Carbon and Metal Surfaces, Langmuir 20 (2004) 8243-8253. https://doi.org/10.1021/la049194c.

[47] T. Peng, D. Zhao, K. Dai, W. Shi, K. Hirao, Synthesis of Titanium Dioxide Nanoparticles with Mesoporous Anatase Wall and High Photocatalytic Activity, J. Phys. Chem. B 109 (2005) 4947-4952. https://doi.org/10.1021/jp044771r.
[48] B.K. Mutuma, G.N. Shao, W.D. Kim, H.T. Kim, Sol–gel synthesis of mesoporous anatase–brookite and anatase–brookite–rutile TiO_2 nanoparticles and their photocatalytic properties, J. Colloid Interface Sci. 442 (2015) 1-7. https://doi.org/10.1016/j.jcis.2014.11.060.
[49] G. Zhang, G. Kim, W. Choi, Visible light driven photocatalysis mediated via ligand-to-metal charge transfer (LMCT): an alternative approach to solar activation of titania, Energy Environ. Sci 7 (2014) 954-966. http://dx.doi.org/10.1039/C3EE43147A.
[50] Y. Liu, D. Zhang, Y. Shang, W. Zang, M. Li, Construction of multifunctional films based on graphene–TiO_2 composite materials for strain sensing and photodegradation, RSC Advances 5 (2015) 104785-104791. http://dx.doi.org/10.1039/C5RA21364A.
[51] X. Min, F. Jiang, F. Qin, Z. Li, J. Tong, S. Xiong, W. Meng, Y. Zhou, Polyethylenimine Aqueous Solution: A Low-Cost and Environmentally Friendly Formulation to Produce Low-Work-Function Electrodes for Efficient Easy-to-Fabricate Organic Solar Cells, ACS Appl. Mater. Interfaces 6 (2014) 22628-22633. https://doi.org/10.1021/am5077974.
[52] B. Sun, W. Hong, E.S. Thibau, H. Aziz, Z.-H. Lu, Y. Li, Polyethylenimine (PEI) As an Effective Dopant To Conveniently Convert Ambipolar and p-Type Polymers into Unipolar n-Type Polymers, ACS Appl. Mater. Interfaces 7 (2015) 18662-18671. https://doi.org/10.1021/acsami.5b05097.
[53] M.a.J. Climent, A. Corma, S. Iborra, A. Velty, Designing the adequate base solid catalyst with Lewis or Bronsted basic sites or with acid–base pairs, J. Mol. Catal. A: Chem. 182-183 (2002) 327-342. https://doi.org/10.1016/S1381-1169(01)00501-5.
[54] G. Li, J. Xiao, W. Zhang, Knoevenagel condensation catalyzed by a tertiary-amine functionalized polyacrylonitrile fiber, Green Chem. 13 (2011) 1828-1836. http://dx.doi.org/10.1039/C0GC00877J.
[55] S.L. Hruby, B.H. Shanks, Acid–base cooperativity in condensation reactions with functionalized mesoporous silica catalysts, J. Catal. 263 (2009) 181-188. https://doi.org/10.1016/j.jcat.2009.02.011.
[56] J. Lauwaert, E. De Canck, D. Esquivel, P. Van Der Voort, J.W. Thybaut, G.B. Marin, Effects of amine structure and base strength on acid–base cooperative aldol condensation, Catal. Today 246 (2015) 35-45. https://doi.org/10.1016/j.cattod.2014.08.007.
[57] A. De Vylder, J. Lauwaert, D. Esquivel, D. Poelman, J. De Clercq, P. Van Der Voort, J.W. Thybaut, The role of water in the reusability of aminated silica catalysts for aldol reactions, J. Catal. 361 (2018) 51-61. https://doi.org/10.1016/j.jcat.2018.02.016.
[58] C. Yu, J. He, Synergic catalytic effects in confined spaces, Chem. Commun. 48 (2012) 4933-4940. http://dx.doi.org/10.1039/C2CC31585H.
[59] D. Appelhans, H. Komber, M.A. Quadir, S. Richter, S. Schwarz, J. van der Vlist, A. Aigner, M. Müller, K. Loos, J. Seidel, K.-F. Arndt, R. Haag, B. Voit, Hyperbranched PEI with Various Oligosaccharide Architectures: Synthesis, Characterization, ATP Complexation, and Cellular Uptake Properties, Biomacromolecules 10 (2009) 1114-1124. https://doi.org/10.1021/bm801310d.
[60] D.R. Holycross, M. Chai, Comprehensive NMR Studies of the Structures and Properties of PEI Polymers, Macromolecules 46 (2013) 6891-6897. https://doi.org/10.1021/ma4011796.
[61] N. Al-Haq, R. Ramnauth, S. Kleinebiekel, D. Li Ou, A.C. Sullivan, J. Wilson, Aminoalkyl modified polysilsesquioxanes; synthesis, characterisation and catalytic activity in comparison to related aminopropyl modified silicas, Green Chem. 4 (2002) 239-244. http://dx.doi.org/10.1039/B200806H.
[62] L.W. Xu, M.S. Yang, J.X. Jiang, H.Y. Qiu, G.Q. Lai, Ionic liquid-functionalized SBA-15 mesoporous material: efficient heterogeneous catalyst in versatile organic reactions, Cent. Eur. J. Chem 5 (2007) 1073-1083. https://doi.org/10.2478/s11532-007-0044-6.

[63] A. Wang, X. Liu, Z. Su, H. Jing, New magnetic nanocomposites of ZrO_2–Al_2O_3–Fe_3O_4 as green solid acid catalysts in organic reactions, Catal Sci Technol 4 (2014) 71-80. http://dx.doi.org/10.1039/C3CY00572K.

Versatile Titanium Dioxide Nanoparticles prepared by Surface-Grown Polymerization of Polyethylenimine for Photodegradation and Catalytic C-C Bond Forming Reactions

Josefa Ortiz-Bustos[a], Mariano Fajardo[a], Isabel del Hierro[a]*, Yolanda Pérez[a]*
Departamento de Biología y Geología, Física y Química Inorgánica. Escuela Superior de Ciencias Experimentales y Tecnología. Universidad Rey Juan Carlos. 28933 Móstoles (Madrid), Spain. Tel.: (+34) 916647444
E-mail: yolanda.cortes@urjc.es

Supplementary Material

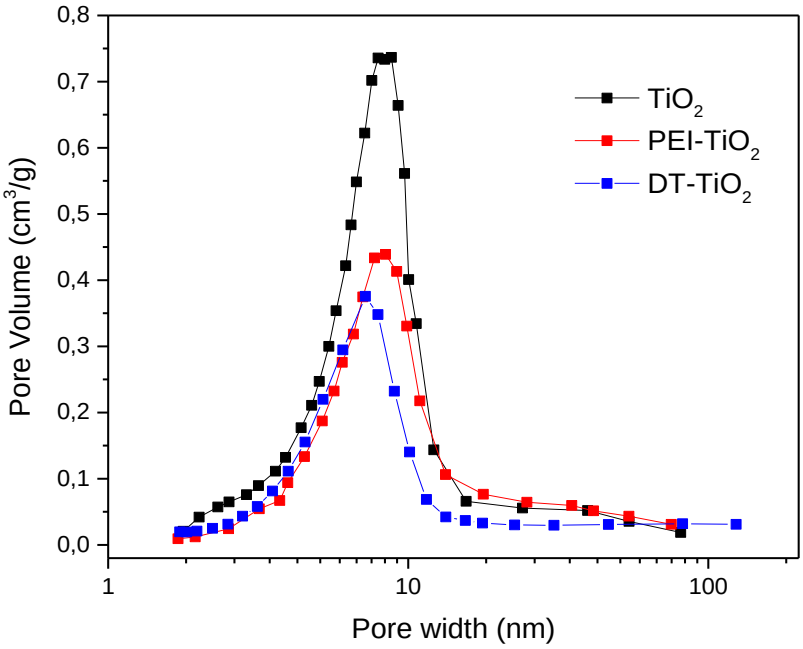

Figure S1. Pore size distribution for TiO_2, DT-TiO_2 and PEI-TiO_2

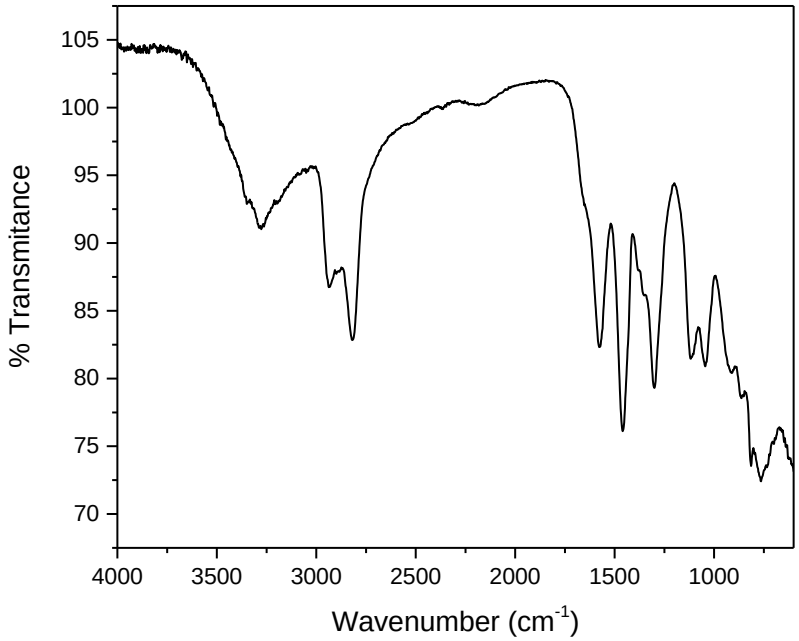

Figure S2. FT-IR spectrum of commercial PEI

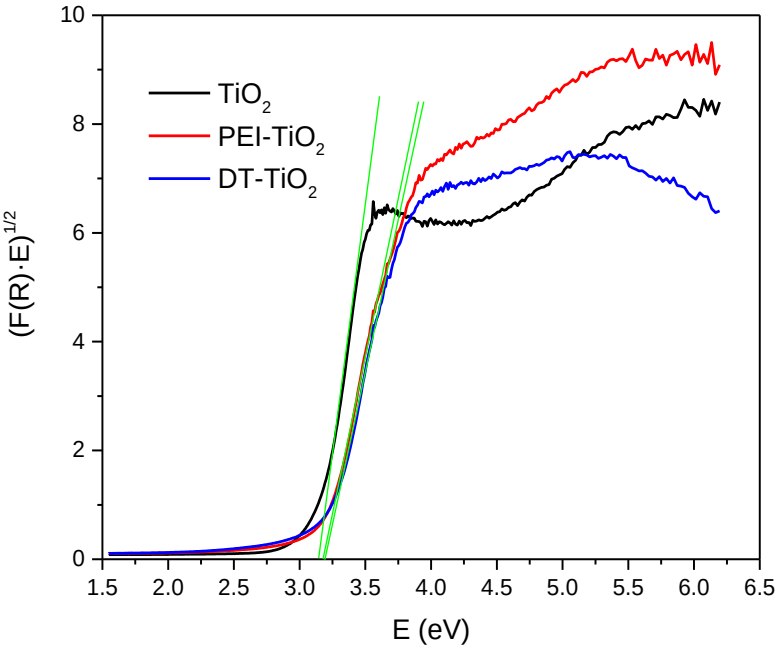

Figure S3. Band gap calculation of TiO_2, DT-TiO_2 and PEI-TiO_2.

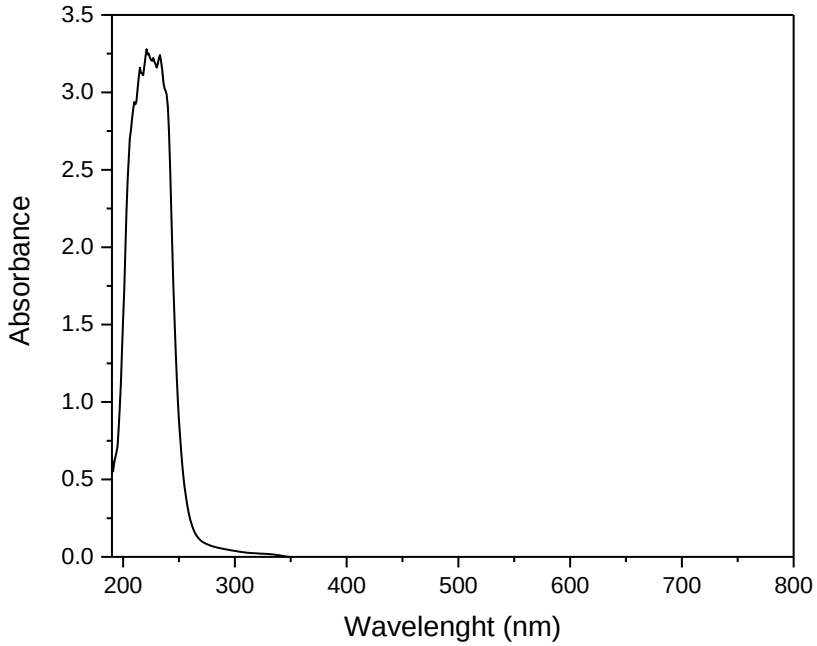

Figure S4. UV-vis spectrum of commercial PEI in ethanol solution

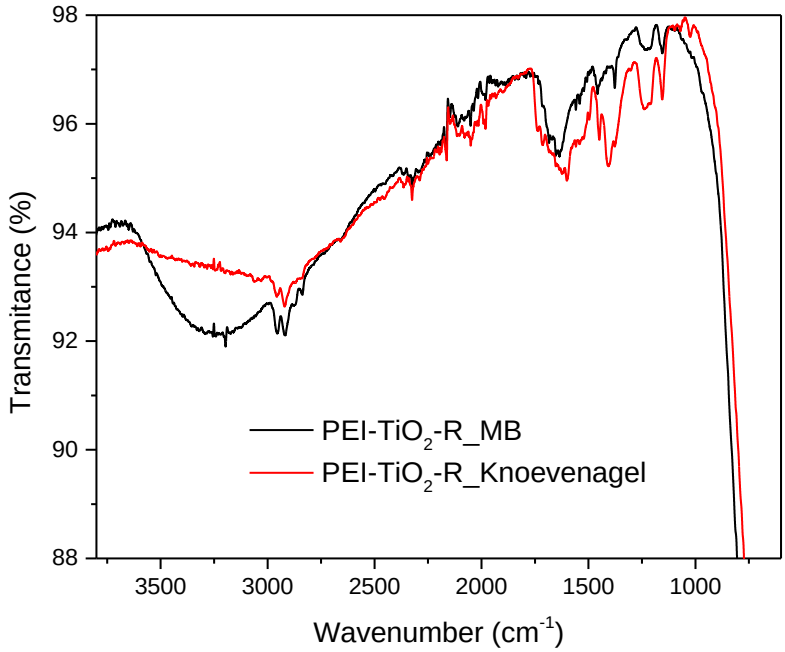

Figure S5. IR spectra of recovered PEI-TiO_2 material after degradation reaction (black plot) and Knoevenagel condensation reaction (red plot).

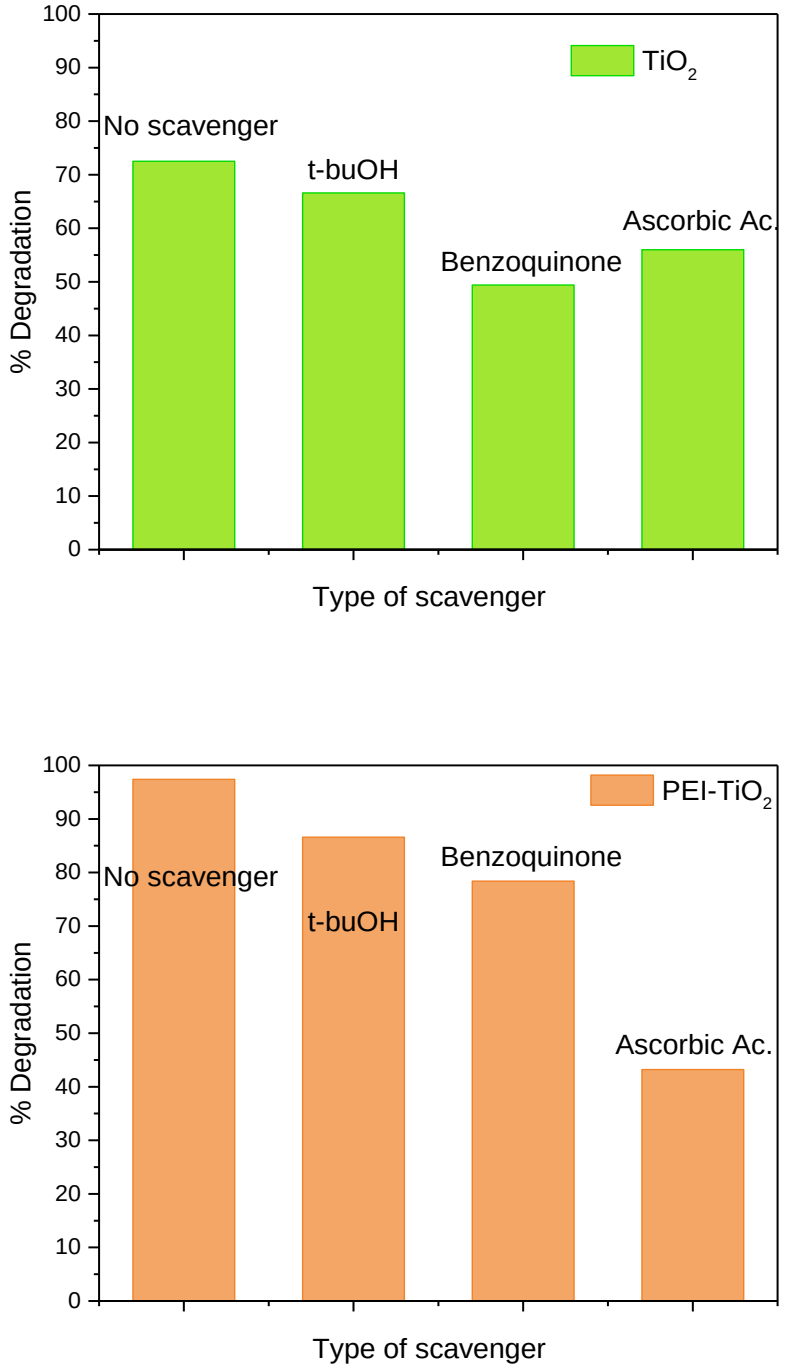

Fig S6. Influence of several types of scavengers on the photocatalytic degradation of MB with TiO_2 and PEI-TiO_2.

Knoevenagel condensation products:

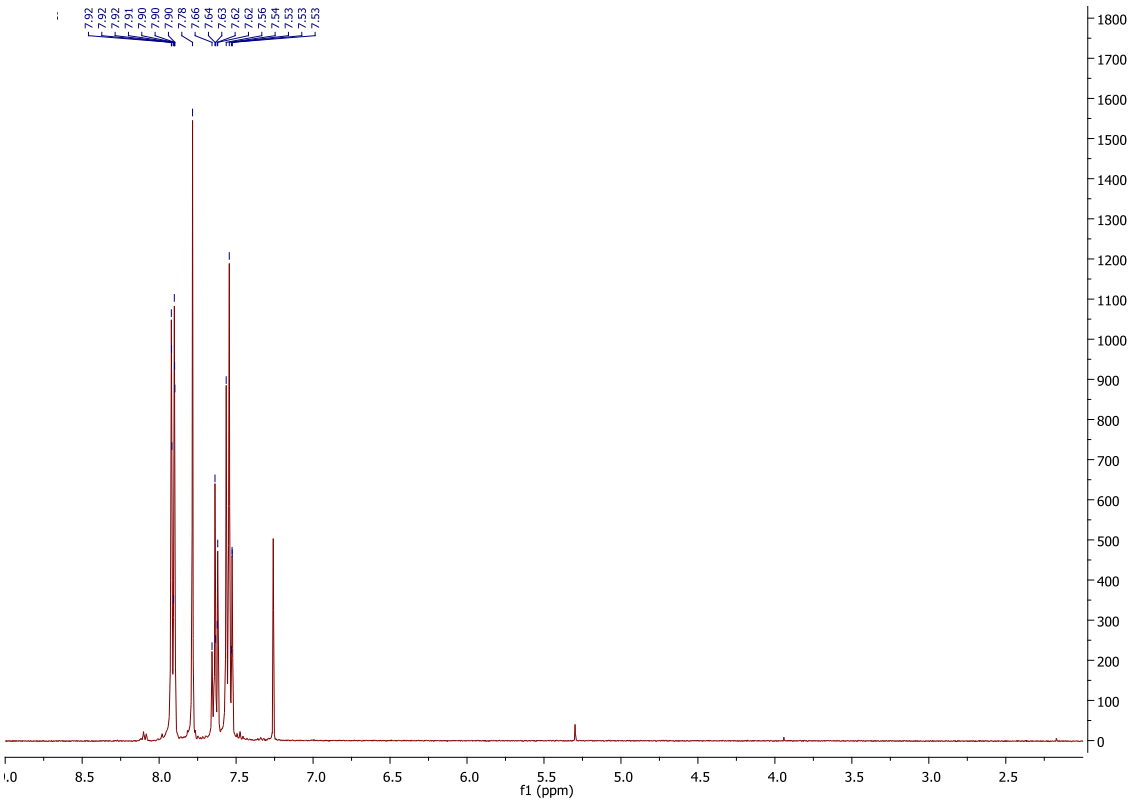

Fig. S7a. ^{1}H NMR spectrum of 2-Benzylidenepropanedinitrile in $CDCl_3$ (Entry 1)

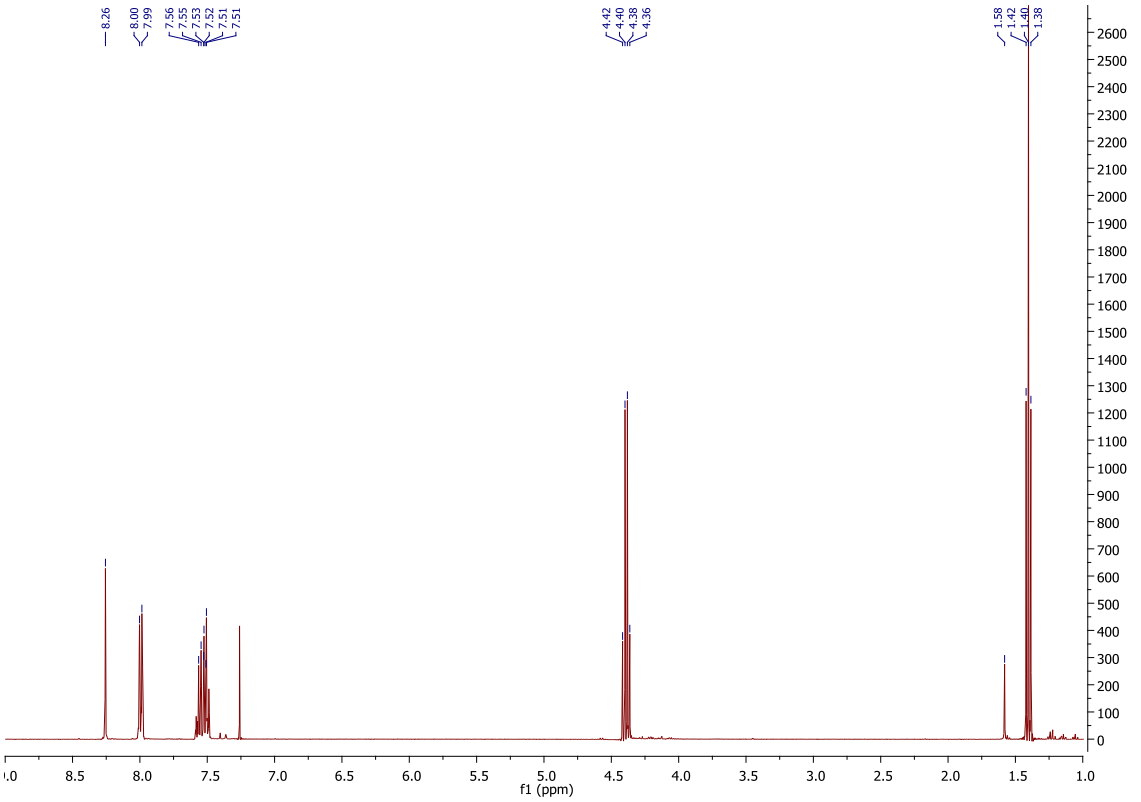

Fig. S7b. ^{1}H NMR spectrum of Ethyl (2E)-2-cyano-3-phenylprop-2-enoate in $CDCl_3$ (Entries 2-17)

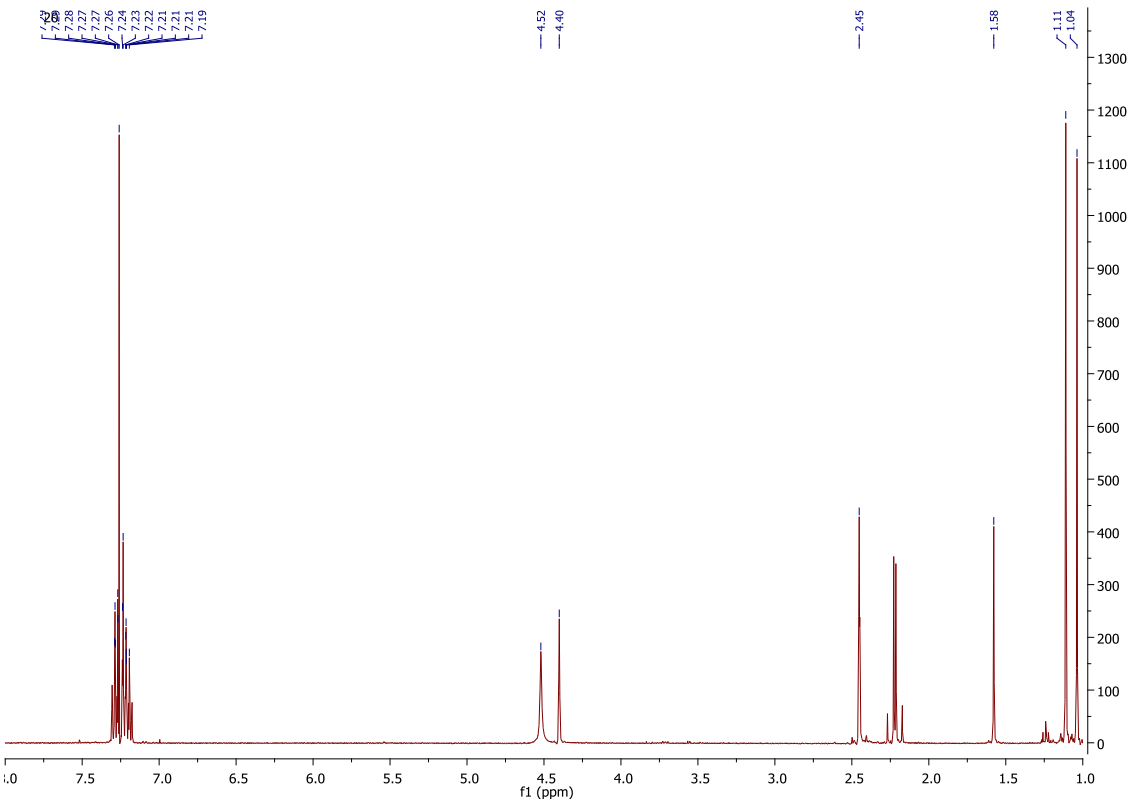

Fig. S8. ^{1}H NMR spectrum of 2-amino-7,7-dimethyl-5-oxo-4-phenyl-5,6,7,8-tetrahydro-4H-chromene-3-carbonitrile (Entries 18-20):

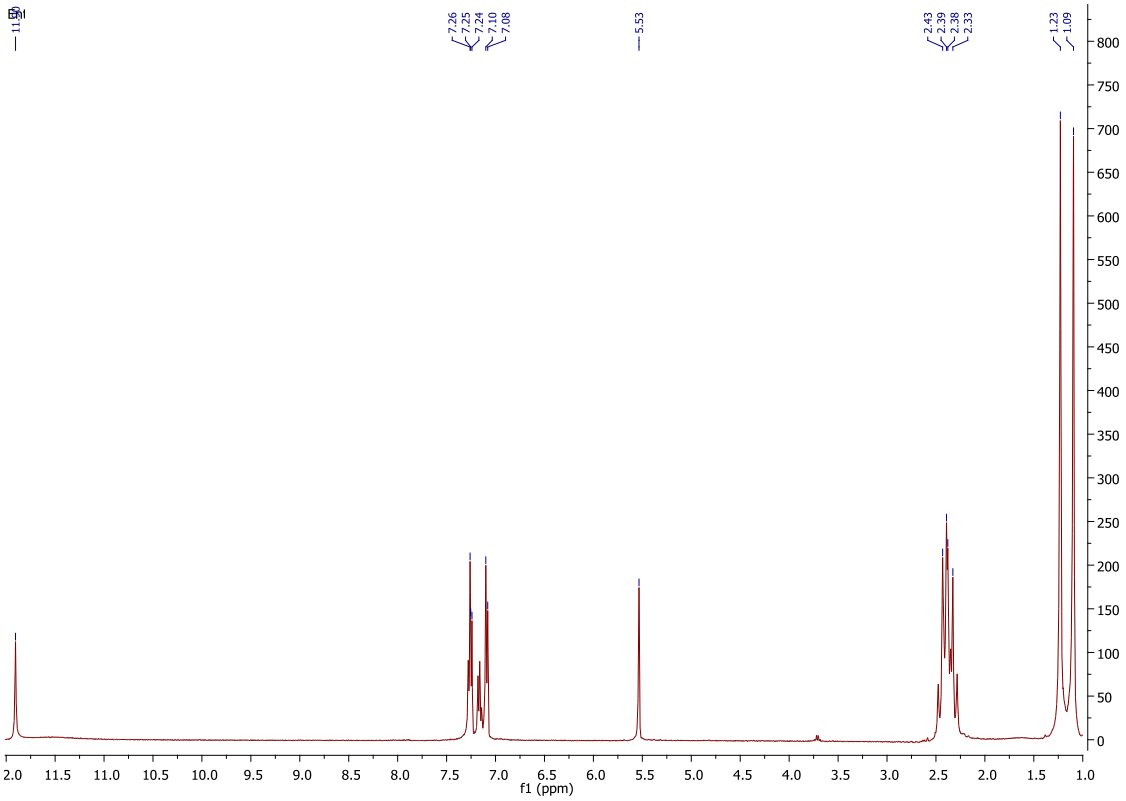

Fig. S9. ^{1}H NMR spectrum of 2,2’-(phenylmethylene)bis(3-hydroxy-5,5-dimethylcyclohex-2-enone) (Entry 21):

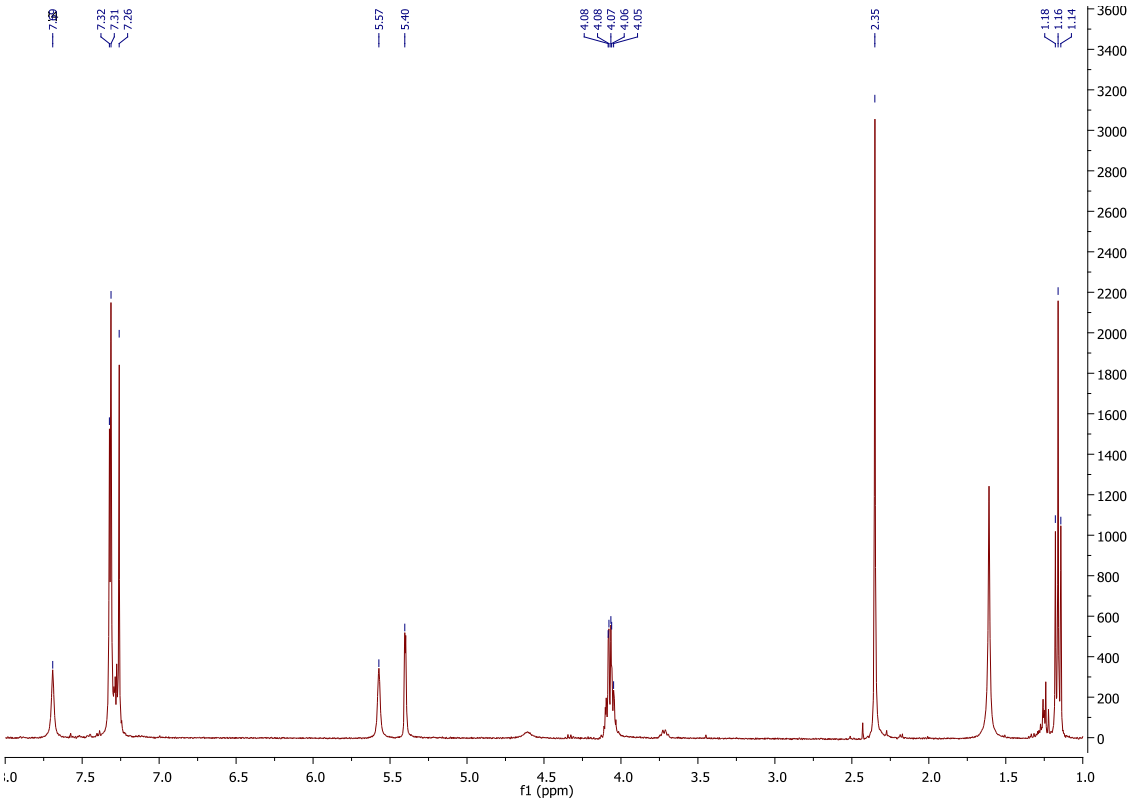

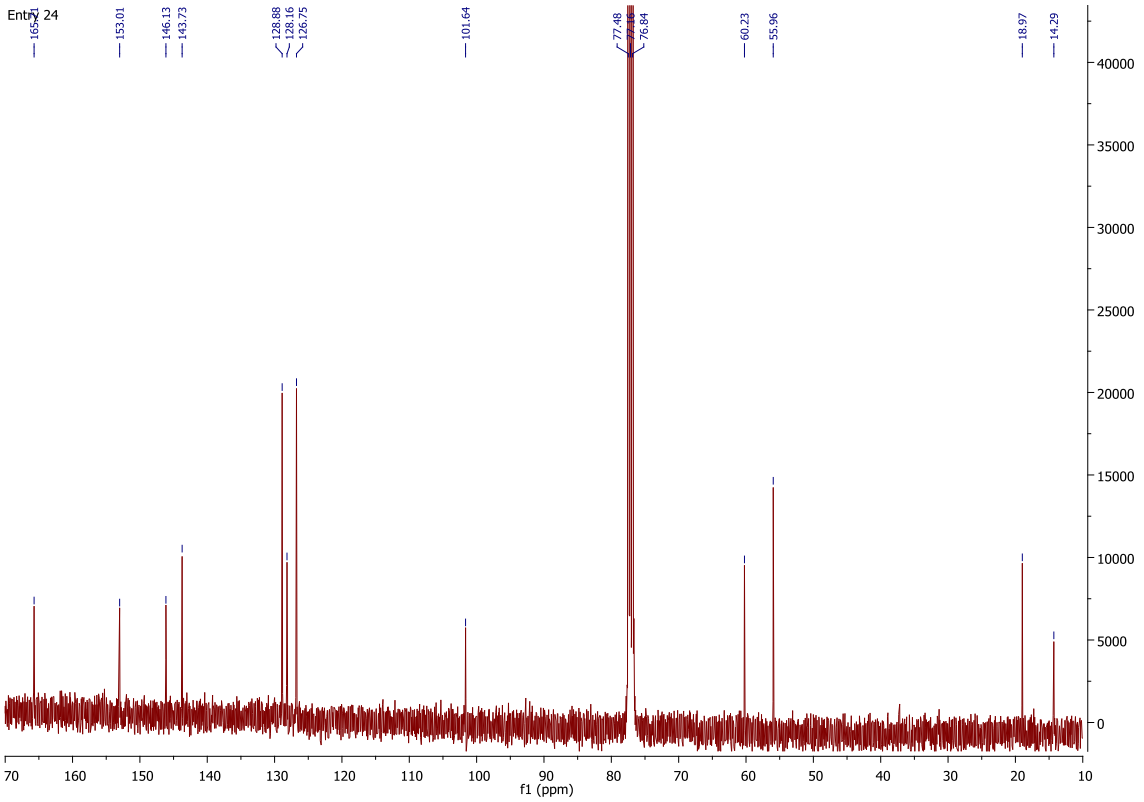

Fig. S10. ^{1}H NMR and ^{13}C spectra of 5-Etoxycarbonyl-4-phenyl-6-methyl-3,4-dihydropyridin-2(1H)-one (Entries 22 and 23)

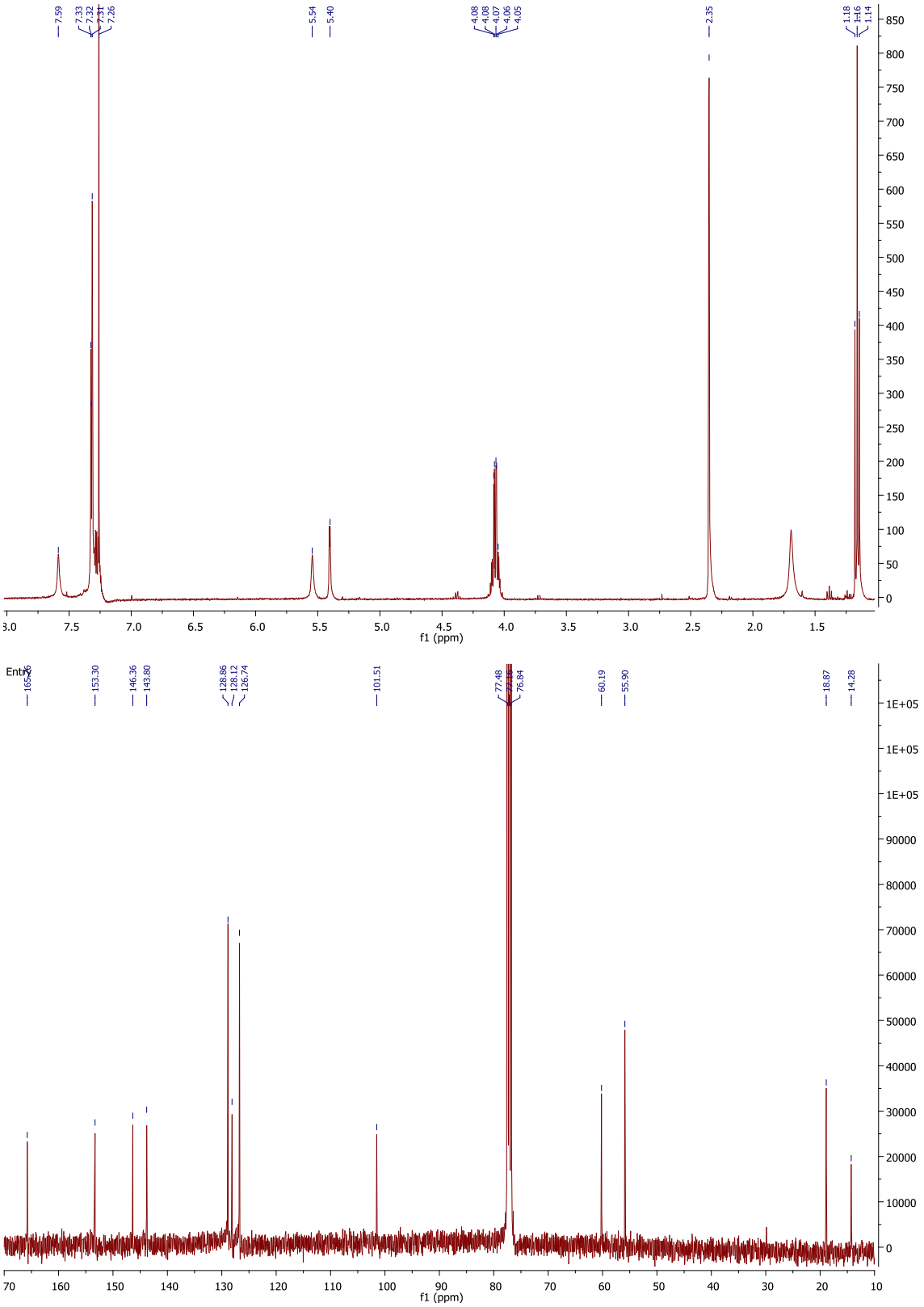

Fig. S11. ^{1}H NMR and ^{13}C NMR spectra of 5-Etoxycarbonyl-4-phenyl-6-methyl-3,4-dihydropyridin-2(1H)-thione (Entries 24 and 25).

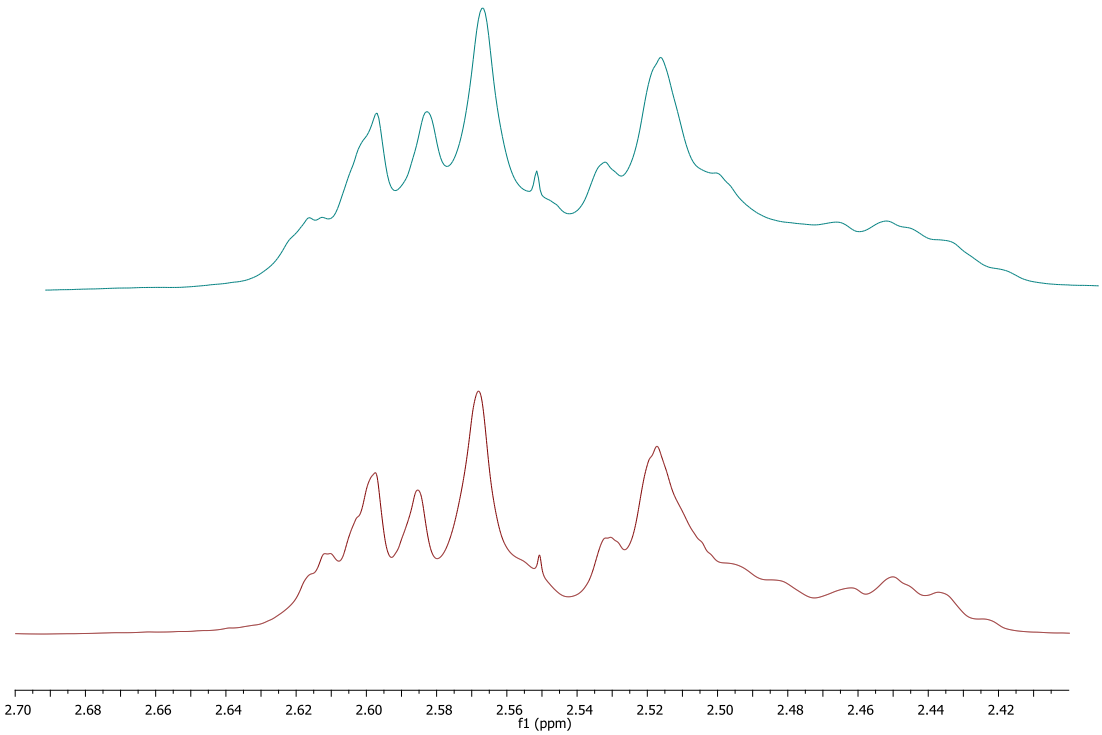

Figure S12. ^{1}H RMN spectra of commercial PEI before (red line) and after (blue line) reaction conditions.